https://doi.org/10.1093/plphys/kiad047 PLANT PHYSIOLOGY 2023: 191: 2534–2550

Plant Physiology®

Research Article

Resting cytosol Ca^{2+} level maintained by Ca^{2+} pumps affects environmental responses in Arabidopsis

Zhan Li,[1,†] Jeffrey F. Harper,[2] Chrystle Weigand[2] and Jian Hua[1,*]

1 School of Integrative Plant Science, Plant Biology Section, Cornell University, Ithaca, NY 14853, USA
2 Department of Biochemistry and Molecular Biology, University of Nevada, Reno, NV 89557, USA
† Present address: Guangdong Provincial Key Laboratory of Plant Molecular Breeding, State Key Laboratory for Conservation and Utilization of Subtropical Agro-Bioresources, South China Agricultural University, Guangzhou, China

*Author for correspondence: jh299@cornell.edu

J.H. conceived and supervised the project; Z.L. performed the experiments and analyzed data; J.F.H. contributed to design and discussion of experiments; C.W. contributed to material generation; Z.L., J.H., and J.F.H. wrote the manuscript.
The author responsible for distribution of materials integral to the findings presented in this article in accordance with the policy described in the Instructions for Authors (https://academic.oup.com/plphys/pages/General-Instructions) is Jian Hua (jh299@cornell.edu).

Abstract

Calcium ion transporting systems control cytosol Ca^{2+} levels ($[Ca^{2+}]_{cyt}$) and generate transient calcium (Ca^{2+}) signatures that are key to environmental responses. Here, we report an impact of resting $[Ca^{2+}]_{cyt}$ on plants from the functional study of calmodulin-regulated Ca^{2+} pumps or Ca^{2+}-ATPases in Arabidopsis (*Arabidopsis thaliana*). The plasma membrane-localized pumps ACA8 (autoinhibited Ca^{2+}-ATPase) and ACA10, as well as the vacuole-localized pumps ACA4 and ACA11, were critical in maintaining low resting $[Ca^{2+}]_{cyt}$ and essential for plant survival under chilling and heat-stress conditions. Their loss-of-function mutants *aca8 aca10* and *aca4 aca11* had autoimmunity at normal temperatures, and this deregulated immune activation was enhanced by low temperature, leading to chilling lethality. Furthermore, these mutants showed an elevated resting $[Ca^{2+}]_{cyt}$, and a reduction of external Ca^{2+} lowered $[Ca^{2+}]_{cyt}$ and repressed their autoimmunity and cold susceptibility. The *aca8 aca10* and the *aca4 aca11* mutants were also susceptible to heat, likely resulting from more closed stomata and higher leaf surface temperature than the wild type. These observations support a model in which the regulation of resting $[Ca^{2+}]_{cyt}$ is critical to how plants regulate biotic and abiotic responses.

Introduction

Calcium (Ca^{2+}) signaling is a critical regulatory process for growth and development as well as environmental responses in plants (Dodd et al. 2010; Kim et al. 2010; Lee and Seo 2021). Environmental stimuli induce specific calcium (Ca^{2+}) signals for corresponding cellular responses. These calcium signals are generated/coded by calcium transporting systems and decoded by a vast variety of calcium-binding signaling proteins (Kudla et al. 2010). The cytoplasmic Ca^{2+} concentration ($[Ca^{2+}]_{cyt}$) is kept at a low concentration under resting state so that a transient calcium signal with unique Ca^{2+} dynamics specific to the stimulus can be generated to serve as a second messenger (Lecourieux et al. 2006; Choi et al. 2016; Luan and Wang 2021). The $[Ca^{2+}]_{cyt}$ is regulated by calcium influx and efflux transporters including calcium ion channels, pumps, and exchangers. Influx channels on the plasma membrane (PM) include cyclic nucleotide-gated channels, glutamate-like receptors, and reduced hyper Osmolality-induced Ca^{2+} increase (Ali et al. 2005; Zhi Qi and Spalding 2006; Yuan et al. 2014; Demidchik et al. 2018). Some of the Ca^{2+} permeable channels have been shown to be involved in the generation of Ca^{2+} signatures in response to biotic and abiotic stresses (Toyota et al. 2018; Tian et al. 2019; Thor et al. 2020). Ca^{2+} efflux systems include low-affinity and high-capacity Ca^{2+}/H^{+} antiporters (CAXs) as well as high-affinity and low-capacity calcium pumps, namely calcium ATPases (Dodd et al. 2010; Kudla et al. 2010). Calcium pumps are

Received November 18, 2022. Accepted December 26, 2022. Advance access publication January 30, 2023

either endoplasmic reticulum (ER)-type ATPases (ECAs or P2A ATPases) or autoinhibited Ca^{2+} ATPases (ACAs or P2B ATPases) (Sze et al. 2000; Spalding and Harper 2011; Garcia Bossi et al. 2020). The activity of ACA is self-inhibited by its N-terminal auto-inhibitory domain (Malmström et al. 1997; Harper et al. 1998), and this inhibition is relieved by its binding to Ca^{2+}/calmodulin (Tidow et al. 2012). Therefore, Ca^{2+} efflux systems could be regulated by environmental signals that modulate cytosolic Ca^{2+} concentrations.

Arabidopsis (*Arabidopsis thaliana*) has 10 ACA type of Ca^{2+} pumps that transport Ca^{2+} out from cytosol to the other compartments. ACA1, ACA2, and ACA7 are localized on the ER (Hong 1999; Rahmati Ishka et al. 2021); ACA4 and ACA11 are localized on the vacuole (Geisler et al. 2000; Lee et al. 2007), while ACA8, ACA9, ACA10, ACA12, and ACA13 are localized on the PM (Bonza et al. 2000; Frei dit Frey et al. 2012; Iwano et al. 2014; Limonta et al. 2014). ACA proteins have been shown to regulate rosette growth, pollen growth, and immune responses in Arabidopsis. The loss-of-function (LOF) mutant of the ER-localized ACAs *aca1 aca2 aca7* had reduced rosette growth in Arabidopsis (Rahmati Ishka et al. 2021). The LOF mutants of PM-localized ACAs, such as *aca10* in the No-0 background and *aca8 aca10* in the Col-0 background, had reduced growth of rosette and inflorescence (George et al. 2008; Frei dit Frey et al. 2012; Yang et al. 2017). The LOF of *ACA13* or *ACA12* did not lead to overt defect but enhanced the defects of *aca8 aca10*, indicating a relatively minor role of ACA12 and ACA13 among the PM-localized ACAs (Yu et al. 2018). Reduced pollen tube growth was reported for the LOF of *ACA9* or *ACA1*, *ACA2*, and *ACA7* together in the pollen (Schiott et al. 2004; Rahmati Ishka et al. 2021) or *ACA13* in papilla cells (Iwano et al. 2014). In addition, the LOF mutants *aca1 aca2 aca7*, *aca4 aca11*, and *aca8 aca10* each exhibited constitutive defense responses in the absence of pathogen infection (namely autoimmune responses) and had enhanced resistance to bacterial pathogens (Boursiac et al. 2010; Yang et al. 2017; Hilleary et al. 2020; Rahmati Ishka et al. 2021). The *aca1 aca2 aca7* and the *aca4 aca11* mutants exhibited a salicylic acid (SA)-dependent cell death in leaves (Boursiac et al. 2010; Rahmati Ishka et al. 2021). Interestingly, rosette growth inhibition in mutants *aca10* (*compact inflorescence 1 cif1*), *aca1 aca2 aca7*, and the *aca4 aca11* results from autoimmune responses, and reduced rosette growth could be largely rescued by blocking of SA biosynthesis or immune signaling (Boursiac et al. 2010; Yang et al. 2017; Rahmati Ishka et al. 2021). Interestingly, *ACA10* and *ACA12* are recently shown to maintain leaf excitability during insect attack and protect leaves from caterpillar damage (Fotouhi et al. 2022).

At the cellular level, ACAs have been reported to affect calcium signals in response to environmental stimuli. The *aca1 aca2 aca7* mutant had a higher magnitude and duration of Ca^{2+} transient signals in response to blue-light and pathogen compared to the wild type (Rahmati Ishka et al. 2021). The *aca4 aca11* mutant showed a higher magnitude Ca^{2+} signal in response to the pathogen elicitor flg22 compared to the wild type (Hilleary et al. 2020). The loss of either *ACA8* or *ACA10* function was reported to abolish calcium oscillations indued by external calcium in the guard cells (Yang et al. 2017). The *aca8 aca10* mutant had a reduced Ca^{2+} increase and slower recovery in response to external ATP in root tip cells compared to the wild type (Behera et al. 2018). In addition to affecting transient calcium signals, ACAs have also been found to affect resting $[Ca^{2+}]_{cyt.}$ The mutants of *aca1 aca2 aca7*, *aca4 aca11*, and *aca8* were reported to have elevated resting $[Ca^{2+}]_{cyt}$ levels without environmental stimuli (Costa et al. 2017; Hilleary et al. 2020; Rahmati Ishka et al. 2021).

Despite these advances, we still lack a clear understanding of the cellular functions of ACA calcium pumps in calcium regulation, their physiological functions in environmental responses, or the connection of cellular function with physiological functions. We started to address these questions by investigating the cellular and physiological function of 2 major PM-localized ACAs (ACA8 and ACA10) and 2 vacuole-localized ACAs (ACA4 and ACA11) in Arabidopsis. These genes have been shown to positively regulate rosette growth and negatively regulate plant immunity. Here, we show that the PM-localized pumps ACA8 and ACA10, as well as the vacuolar-localized pumps ACA4 and ACA11, are important for maintaining low resting $[Ca^{2+}]_{cyt}$ levels and that elevated resting $[Ca^{2+}]_{cyt}$ levels are largely responsible for the triggering autoimmunity as well as chilling lethality and heat lethality. This study thus emphasizes the importance of resting $[Ca^{2+}]_{cyt}$ in regulating both biotic and abiotic stress responses as well as the interconnection among defense response and chilling tolerance.

Results

ACA8 and *ACA10* maintain a low resting $[Ca^{2+}]_{cyt}$ in cells

We used a ubiquitously expressed and highly sensitive Ca^{2+} indicator GCaMP6s to monitor $[Ca^{2+}]_{cyt}$ in the *aca8 aca10* mutant as previously described (Yang et al. 2017; Yu et al. 2018). This engineered green fluorescent protein (GFP) fusion is capable of changing its conformation and thus fluorescence in a Ca^{2+} concentration-dependent manner (Chen et al. 2013; Liu et al. 2017). The GCaMP6s indicator was introduced into the *aca8 aca10* mutant by *Agrobacterium*-mediated transformation and introgressed into the wild type by hybridization, so that these reporter lines were isogeneic with the GCaMP reporter gene inserted in the identical chromosome location. Confocal microscopy of leaf epidermal pavement cells revealed a higher GCaMP fluorescence in the *aca8 aca10* mutant than in the wild type, which was confirmed by quantification of the fluorescence signals (Fig. 1A). Immunoblot detected the same level of the GCaMP6s protein in the wild-type and the *aca8 aca10* lines (Supplemental Fig. S1A), excluding the possibility that higher reporter protein

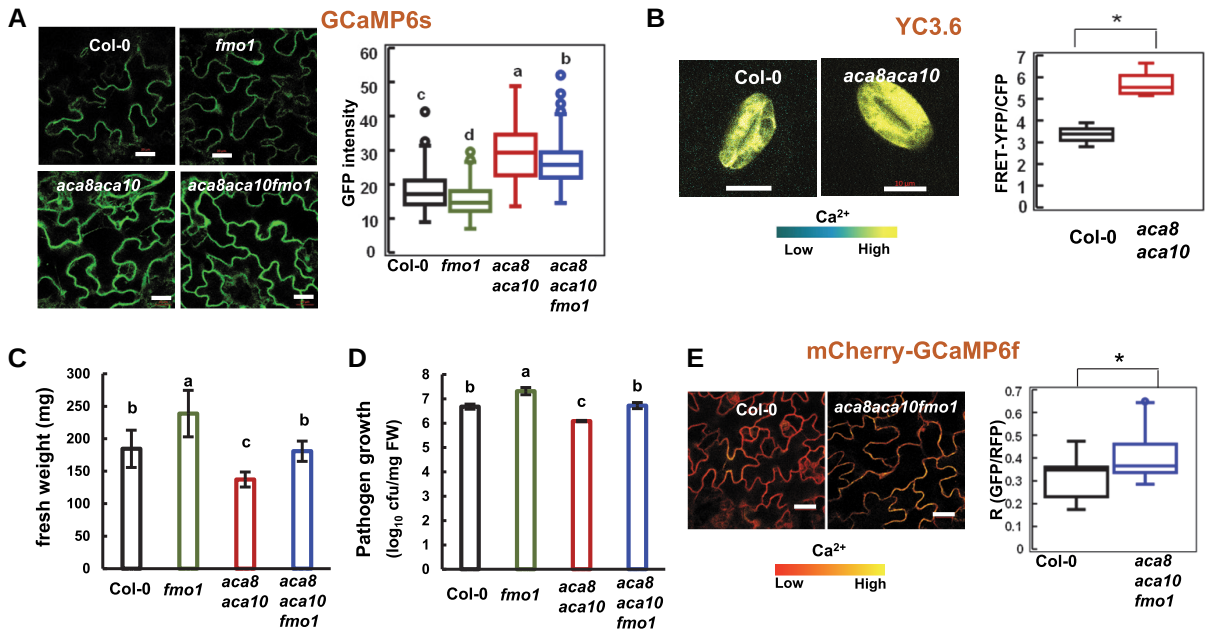

Figure 1. Resting $[Ca^{2+}]_{cyt}$ is elevated in the *aca8 aca10* mutants. A) Images and quantification (in box plot) of GFP fluorescence signals from the reporter GCaMP6s in epidermal cells of isogenic plants of wild-type Col-0, *fmo1*, *aca8 aca10*, and *aca8 aca10 fmo1*. Plants were grown at 22 °C for 21 d. The scale bar is 20 μm. B) Images and quantification (in box plot) of fluorescence signal ratios of FRET-YFP and CFP from the reporter YC3.6 in guard cells of wild-type Col-0 and *aca8 aca10* plants that were grown in soil for 21 d. The scale bar is 10 μm. C) Fresh weights of Col-0, *fmo1*, *aca8 aca10*, and *aca8 aca10 fmo1* plants after grown under constant light for 21 d at 22 °C. Error bars represent standard deviations (SD) from 9 plants for each genotype. D) Growth of virulent pathogen *Pseudomonas syringae* pathovar tomato (*Pst*) DC3000 in Col-0, *fmo1*, *aca8 aca10*, and *aca8 aca10 fmo1* plants grown under a 12/12-h photoperiod for 14 d. Shown are $\log_{10}$ values of bacterial number (in colony forming unit, cfu) per mg fresh weight (FW) of leaves at 3 d after infection. Error bars represent standard deviations (SD) from 3 biological replicates in 1 experiment. Shown is a result from 1 experiment and similar results were obtained from 3 experiments. E) Images and quantification of fluorescence signal ratios GFP/mCherry from the reporter mCherry-GCaMP6f in leaf epidermal cells of the wild-type Col-0 and the *aca8 aca10 fmo1* mutant plants. The scale bar is 20 μm. For A) and E), fluorescence signals were measured from the region of interest of 2 × 2 μm, and the average of signals or signal ratios from 4 regions of interest (ROIs) was used as the signal or signal ratio for one cell. Data were obtained from at least 60 cells (2 cells/plant) for each genotype. For B), fluorescence signals were acquired from a- ROI encompassing the entire guard cell. More than 10 cells (1 cell/plant) for each genotype were measured. For box-whisker plots in A), B), and E), the top and bottom sides of the box are the upper and lower quartiles; the line in the box is the median; the whiskers mark the range from maximum to minimum or 1.5 times the interquartile range with outliers represented as a circle. For B) and E), "*" indicates a statistically significant difference between samples determined by Student's *t*-test ($P < 0.05$). For A), C), and D), different letters indicate significant differences among samples by ANOVA test ($P < 0.05$).

level was the cause of higher fluorescence signal. These data suggested that the *aca8 aca10* mutant had a higher resting $[Ca^{2+}]_{cyt}$ compared to the wild type.

We verified this by using a ratiometric calcium sensor Yellow Cameleon (YC) which is based on calcium-dependent fluorescence resonance energy transfer (FRET) efficiency between cyan fluorescent protein (CFP) and yellow fluorescent protein (YFP) (Nagai et al. 2004). A plant version of the calcium sensor YC3.6 was transformed into *aca8 aca10* and then introduced to the wild type by crossing. The expression of YC3.6 is often silenced in other cell types, so we analyzed confocal images of its signal in guard cells where the reporter is highly expressed. Quantification of ratiometric signals revealed a higher $[Ca^{2+}]_{cyt}$ in the *aca8 aca10* mutant compared with the wild type (Fig. 1B), corroborating the observations with GCaMP6s in pavement cells. The two calcium reporters GCaMP6s and the YC3.6 were effective to detect transient $[Ca^{2+}]_{cyt}$ response to external Ca^{2+} treatment. The GCaMP6s protein level was not altered by external Ca^{2+} treatment in wild-type Col-0 or the *aca8 aca10* mutant (Supplemental Fig. S1C). A similar increase of $[Ca^{2+}]_{cyt}$ in response to external Ca^{2+} treatment was observed in wild-type Col-0 leaves when using the reporters YC3.6 and GCaMP6s (Supplemental Fig. S1B and C).

Elevated resting $[Ca^{2+}]_{cyt}$ in *aca8 aca10* is not due to autoimmunity

Because activation of immune responses could potentially trigger calcium influx (Bi et al. 2021; Jacob et al. 2021), we investigated whether or not the elevated resting $[Ca^{2+}]_{cyt}$ in *aca8 aca10* was an indirect result from autoimmunity (constitutive immune response) in the mutant. A suppressor mutation of *aca8 aca10* was used to differentiate the possibilities. This suppressor was isolated from an ethyl methane sulfonate (Atwell et al. 2010) mutagenesis of the *aca8 aca10* mutant

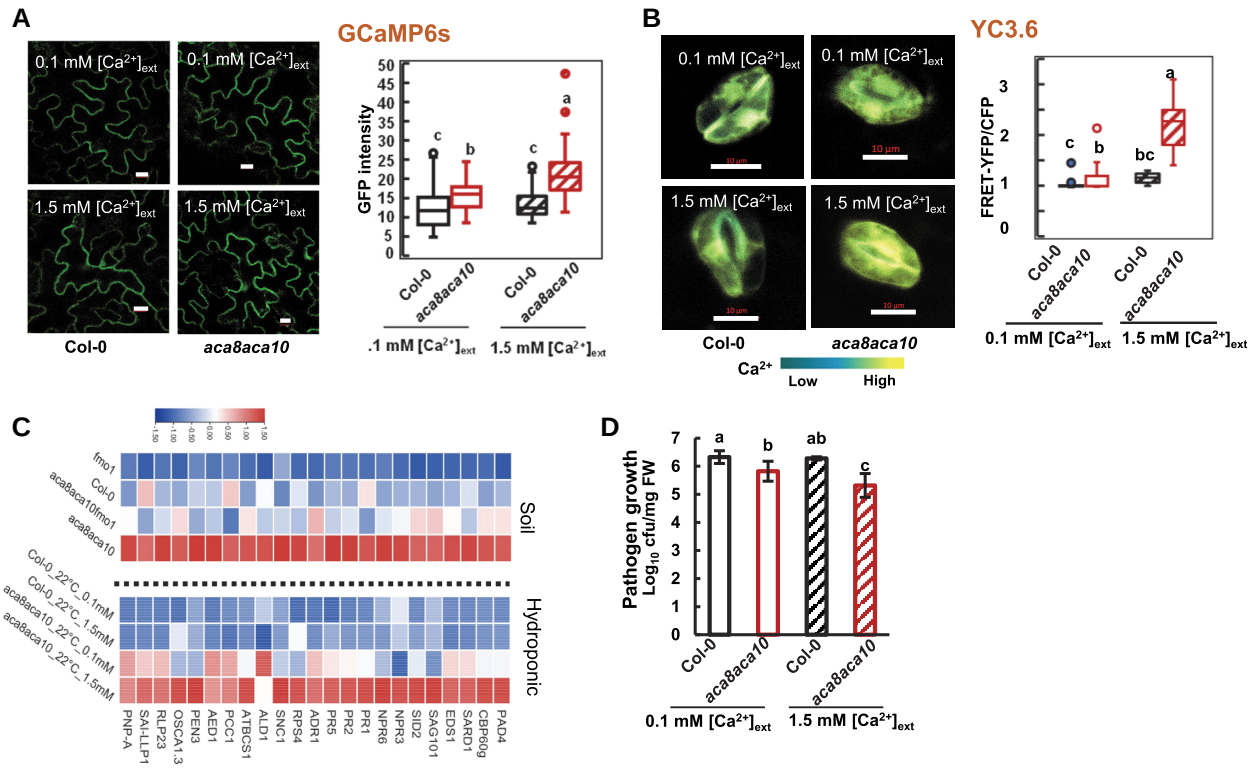

Figure 2. Low $[Ca^{2+}]_{ext}$ reduces autoimmunity in *aca8 aca10* mutants. A) Images and quantification (in box plot) of fluorescence signals from GCaMP6s in leaf epidermal cells of isogenic plants of wild-type Col-0 and *aca8 aca10* containing the reporter gene. Plants were hydroponically grown under 0.1 or 1.5 mM $[Ca^{2+}]_{ext}$ at 22 °C with constant light for 21 d. The scale bar is 10 µm. The average of fluorescence signals measured from 4 regions of interest (ROIs) (each at 2 × 2 µm) was used as the signal for one epidermal cell. More than 10 cells (1 cell/plant) for each genotype were measured. B) Images and quantification (in box plot) of fluorescence signal ratios of FRET-YFP and CFP from the reporter YC3.6 in guard cells of isogenic wild-type Col-0 and *aca8 aca10* plants grown hydroponically at 22 °C (scale bar, 10 µm). Fluorescence signals were acquired from a ROI encompassing the entire guard cell. More than 15 cells (1 cell/plant) for each genotype were measured. C) Heatmap showing relative expression of defense-related genes in plants of wild-type Col-0, *fmo1*, *aca8 aca10*, and *aca8 aca10 fmo1* grown either in soil or hydroponically under 0.1 or 1.5 mM $[Ca^{2+}]_{ext}$. D) Growth of *Pst* DC3000 in wild-type Col-0 and *aca8 aca10* plants hydroponically grown under 0.1 and 1.5 mM $[Ca^{2+}]_{ext}$ at 22 °C. Seedlings were grown under a 12/12-h photoperiod for 14 d before they were infected. Shown is the $\log_{10}$ value of the bacterial number (in colony forming unit, cfu) per mg fresh weight (FW) in leaves at 3 d after infection in one representative experiment. Error bars represent SD from 3 biological replicates. Similar results were obtained from 3 independent experiments (each with 3 biological repeats). For box-whisker plots in A) and B), the top and bottom sides of the box are the upper and lower quartiles; the line in the box is the median; the whiskers mark the range from maximum to minimum or 1.5 times the interquartile range with outliers represented as a circle. For A), B), and D), different letters indicate statistically significant differences tested by ANOVA ($P < 0.05$).

based on its reversion to the wild-type growth morphology (Supplemental Fig. S1E). Mapping-by-sequencing of the suppressor mutant revealed a stop gain mutation at the nucleotide position of 1378 relative to the translation start site of the *flavin-dependent-monooxygenase1* (*FMO1*) gene which is crucial for systemic-acquired resistance (Hartmann et al. 2018), and the suppressor mutant was, therefore, named as *fmo1-2* (Supplemental Fig. S1D). The *aca8 aca10 fmo1-2* mutant, unlike *aca8 aca10*, had a similar growth to the wild-type Col-0 (Fig. 1C, Supplemental Fig. S1E) and was as susceptible as the wild-type Col-0 to the virulent pathogen *Pseudomonas syringae* pathovar tomato (*Pst*) strain DC3000 (Fig. 1D). The identity of *FMO1* as the suppressor gene of both the growth and immunity defects of the *aca8 aca10* mutant was confirmed by another mutant allele *fmo1* (Alonso et al. 2003) (Fig. 1 C, Supplemental Fig. S1, D–F). Therefore, the *aca8 aca10 fmo1* mutant lacks ACA8 and ACA10 function but has little autoimmunity.

We introduced the GCaMP6s reporter into both the *aca8 aca10 fmo1* and *fmo1* mutants by crossing so that they were isogenic with the GCaMP6s lines of wild type and *aca8 aca10* described above. Expression of the GCaMP6s protein was found to be similar among plants of the wild type, *fmo1*, *aca8 aca10*, and *aca8 aca10 fmo1* (Supplemental Fig. S1A). Confocal imaging of leaf epidermal cells revealed that resting $[Ca^{2+}]_{cyt}$ in *aca8 aca10 fmo1* and in *aca8 aca10* were similar to each other and that both were higher than those in *fmo1* and Col-0 which were similar to each other (Fig. 1A).

The ratiometric calcium reporter mCherry-GCaMP6f (Weigand et al. 2021) was further used to monitor $[Ca^{2+}]_{cyt}$ in the wild-type Col-0 and the *aca8 aca10 fmo1* mutant. $[Ca^{2+}]_{cyt}$ was quantified by the ratio of GFP signal from

GCaMP6f versus red fluorescent protein (RFP) signal from mCherry in transgenic plants containing this reporter. Using this third reporter, the resting $[Ca^{2+}]_{cyt}$ in *aca8 aca10 fmo1* in epidermal cells was also found to be significantly higher in the *aca8 aca10 fmo1* mutant compared to the wild-type Col-0 (Fig. 1E). These data indicate that the high resting $[Ca^{2+}]_{cyt}$ in *aca8 aca10* is not an indirect consequence of autoimmunity but rather a direct effect from the loss of ACA8 and ACA10 function.

Low $[Ca^{2+}]_{ext}$ reduces the elevated $[Ca^{2+}]_{cyt}$ in the *aca8 aca10* mutant

We asked whether or not the high resting $[Ca^{2+}]_{cyt}$ in the *aca8 aca10* mutant is the cause of autoimmunity, the upregulation of defense responses under nonpathogenic conditions. A hydroponic system was used to alter the resting $[Ca^{2+}]_{cyt}$ in the mutant by varying the external Ca^{2+} concentration ($[Ca^{2+}]_{ext}$). Seedlings of the GCaMP6s indicator lines were hydroponically grown in a medium with $[Ca^{2+}]_{ext}$ at 0.1 or 1.5 mM for 21 d before leaves were imaged by confocal microscopy. For the wild type, $[Ca^{2+}]_{cyt}$ in epidermal cells was not significantly different between plants grown under 0.1 and 1.5 mM $[Ca^{2+}]_{ext}$ (Fig. 2A). In contrast, $[Ca^{2+}]_{cyt}$ of the *aca8 aca10* mutant grown in 0.1-mM $[Ca^{2+}]_{ext}$ was significantly lower than when grown in 1.5-mM $[Ca^{2+}]_{ext}$, although still higher than that in the wild type (Fig. 2A). A similar effect was also observed in guard cells by using the ratiometric YC3.6 reporter. No significant difference of $[Ca^{2+}]_{cyt}$ was observed between 0.1 and 1.5 mM $[Ca^{2+}]_{ext}$ for the wild type, while $[Ca^{2+}]_{cyt}$ in the *aca8 aca10* mutant was higher under 1.5 mM $[Ca^{2+}]_{ext}$ than under 0.1 mM $[Ca^{2+}]_{ext}$ (Fig. 2B). This indicates that the wild-type plants maintain a constant low $[Ca^{2+}]_{cyt}$ despite a varying $[Ca^{2+}]_{ext}$ and a low $[Ca^{2+}]_{ext}$ partially alleviated the elevation of resting $[Ca^{2+}]_{cyt}$ in the *aca8 aca10* mutant.

Low $[Ca^{2+}]_{ext}$ reduces autoimmunity in the *aca8 aca10* mutant

In order to reveal the molecular effects of elevated resting $[Ca^{2+}]_{cyt}$ induced by the LOF of ACA8 and ACA10, we analyzed transcriptomes of seedlings of *aca8 aca10* and *aca8 aca10 fmo1* grown in soil as well as *aca8 aca10* seedlings hydroponically grown under 0.1 and 1.5 mM $[Ca^{2+}]_{ext}$. RNAs were extracted from the leaves of these seedlings and were subjected to 3′-RNA seq (Tandonnet and Torres 2017). Cluster analysis on differentially expressed genes (DEGs) on soil-grown plants revealed 6 major groups (G1 to G6) for all DEGs among wild type, *fmo1*, *aca8 aca10*, and *aca8 aca10 fmo1* (Supplemental Fig. S2A). G1 is the largest co-expression group with the highest expression in *aca8 aca10* and the lowest expression in *fmo1* and wild-type Col-0. Most of the enriched Gene Ontology (GO) terms for genes in this group are related to defense responses that include "innate immune response-activating signal transduction," "SA signaling pathway," and "systemic-acquired resistance" (Supplemental Fig. S2B), suggesting that the defense response mediated by SA was activated in the *aca8 aca10* mutant under normal growth conditions without pathogen infection. Found in this group were multiple SA biosynthesis genes including *SID2* and SA signaling genes, such as *EDS1*, *PAD4*, and *CBP60g*, as well as intracellular immune receptor nucleotide-binding and leucine-rich repeat proteins (NLR) genes, such as *RPS4* and *SNC1* (Fig. 2C). A total of 23 genes in these 3 above-mentioned GO terms were selected as markers for autoimmunity in the *aca8 aca10* in subsequent gene expression analysis. As expected, the expression of these defense genes was lower in *fmo1* compared to the wild-type Col-0 and was lower in *aca8 aca10 fmo1* compared to *aca8 aca10* (Fig. 2C, Supplemental Data Set S1).

For hydroponically grown plants under 0.1 and 1.5 mM $[Ca^{2+}]_{ext}$, an upregulation of defense response-related genes was also observed in the *aca8 aca10* mutant. Heat map revealed that these defense response-related genes had a similar expression level under 0.1 and 1.5 mM $[Ca^{2+}]_{ext}$ in the wild type (Fig. 2C, Supplemental Data Set S2). They had a higher expression in *aca8 aca10* compared to the wild type under 1.5 mM $[Ca^{2+}]_{ext}$, similar to soil-grown plants (Fig. 2C). Expression of these genes in *aca8 aca10* was much lower when grown under 0.1 mM $[Ca^{2+}]_{ext}$ compared to grown under 1.5 mM $[Ca^{2+}]_{ext}$, although still higher than in wild type (Fig. 2C). For instance, expression of *SID2* was 2.5-fold higher at 1.5 mM $[Ca^{2+}]_{ext}$ but was reduced to 1.5-fold at 0.1 mM $[Ca^{2+}]_{ext}$ in the *aca8 aca10* mutant compared to wild-type Col-0 (either 0.1 or 1.5 mM $[Ca^{2+}]_{ext}$) (Supplemental Fig. S3F). The effect of reduction of defense gene expression was similar from the *fmo1* mutation and from low $[Ca^{2+}]_{ext}$ (Fig. 2C). This association strongly suggests that a high resting $[Ca^{2+}]_{cyt}$ is responsible for the high expression of defense response genes in *aca8 aca10*.

Low $[Ca^{2+}]_{ext}$ increases pathogen growth in the *aca8 aca10* mutant

We subsequently examined pathogen growth in the *aca8 aca10* mutant that was hydroponically grown under a low $[Ca^{2+}]_{ext}$. Early studies found a reduced growth of virulent pathogen *Pst*DC3000 in soil-grown *aca8 aca10* mutant compared to the wild type (Yang et al. 2017; Yu et al. 2018), likely due to the upregulation of defense response genes even before pathogen infection. The growth of *Pst* DC3000 in wild-type Col-0 seedlings was similar when grown in medium with 0.1 or 1.5 mM $[Ca^{2+}]_{ext}$ (Fig. 2D). The growth of *Pst* DC3000 was reduced by 10-fold under 1.5 mM $[Ca^{2+}]_{ext}$ but by less than 3-fold under 0.1 mM $[Ca^{2+}]_{ext}$ in the *aca8 aca10* mutant compared to the wild type (Fig. 2D). This indicates that a lower $[Ca^{2+}]_{ext}$, resulting in a low $[Ca^{2+}]_{cyt}$, partially reverted the enhanced disease resistance in the *aca8 aca10* mutant. The association between the increased $[Ca^{2+}]_{cyt}$ and the enhanced disease resistance in the mutant further supports that an increase of $[Ca^{2+}]_{cyt}$ is responsible for immune response activation in the *aca8 aca10* mutant.

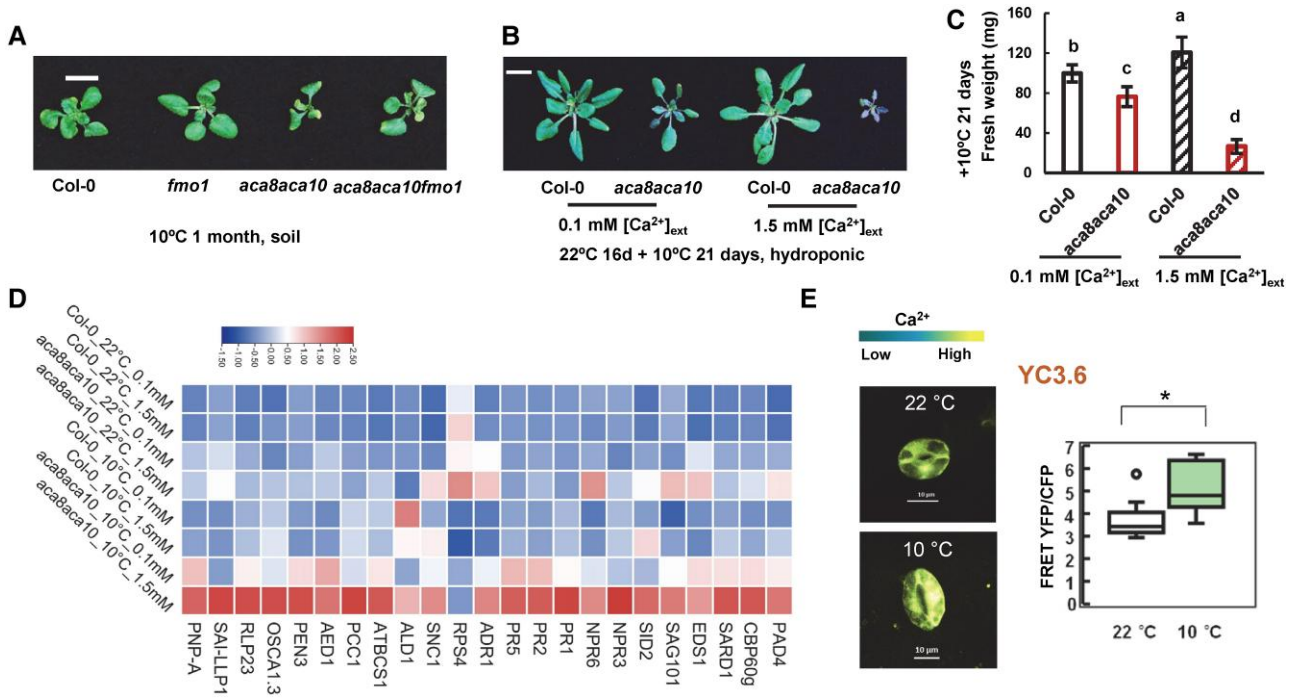

Figure 3. The chilling susceptibility of the *aca8 aca10* mutant is dependent on defense activation and influenced by $[Ca^{2+}]_{ext}$. A) Rosettes of wild-type Col-0, *fmo1*, *aca8 aca10*, and *aca8 aca10 fmo1* plants grown in soil after 1 mo of chilling treatment. Seedlings were germinated and grown at 22 °C for 5 d before chilling treatment at 10 °C (Scale bar, 10 mm). Characterization of chilling phenotypes, including rosette growth B), fresh weight C), and gene expression D), of wild-type Col-0 and *aca8 aca10* plants grown hydroponically under 0.1 and 1.5 mM $[Ca^{2+}]_{ext}$. Seedlings were hydroponically grown for 16 d at 22 °C and then at 10 °C for 21 d. Fresh weight is shown as mean values and SD of more than 30 plants for each genotype and growth condition in C). The scale bar is 10 mm in B). Different letters indicate significant differences among samples by ANOVA test ($P < 0.05$). The expression of a set of defense response genes is displayed as a heatmap in D). E) Images and quantification (in box plot) of fluorescence signal ratios of YFP and CFP from the reporter YC3.6 in guard cells of wild-type Col-0 plants grown at 22 °C or at 10 °C (scale bar, 10 μm). Seedlings were grown at 22 °C for 21 d and kept at 22 °C or moved to10 °C for 5 d. YFP and CFP signals were acquired from a region of interest (ROI) encompassing the entire guard cell. More than 10 cells (1 cell/plant) for each genotype were measured. For the box-whisker plot, the top and bottom sides of the box are the upper and lower quartiles; the line in the box is the median; the whiskers mark the range from maximum to minimum or 1.5 times the interquartile range with outliers represented as a circle. "*" indicates a statistically significant difference between samples determined by Student's *t*-test (*$P < 0.05$).

ACA10 and *ACA8* are crucial for plant survival at low temperatures

To have a more comprehensive understanding of the function of ACA8 and ACA10, we examined their roles and mechanism in coping with abiotic stresses, especially chilling and heat. No functional studies of these genes in temperature stress response have been carried out before, although *ACA8* and *ACA10* were reported to have an altered RNA expression upon chilling treatment (Schiott and Palmgren 2005). The *aca8 aca10* mutant and the wild type were grown in soil for an extended period at a low temperature of 10 °C after germination at 22 °C for 5 d. The wild-type plants had a slower development at 10 °C than at 22 °C, but were able to maintain rosette growth till they bolted at 4 mo (instead of 5 wk at 22 °C). Compared to the wild-type Col-0, the *aca8 aca10* grew even slower at 10 °C, leading to smaller rosettes with fewer leaves (Fig. 3A and Supplemental Fig. S3A). The mutant started to turn yellow after 1 mo of growth at 10 °C, and it eventually died without bolting after 3 mo at 10 °C (Supplemental Fig. S3B). This indicates that *ACA8* and *ACA10* are essential for plant survival at low temperatures.

Autoimmunity contributes to chilling lethality in the *aca8 aca10* mutant

We asked whether or not the lethality of *aca8 aca10* at low temperature was due to a hyper-activation of defense responses as low temperature has been shown to enhance defense responses (Wang et al. 2013). Because the *fmo1* mutation suppressed the defense activation to a large extent in the *aca8 aca10* mutant, the growth phenotype of the *aca8 aca10 fmo1* triple mutant was analyzed at 10 °C. The *aca8 aca10 fmo1* mutant had a larger rosette with more leaves compared to the *aca8 aca10* mutant during the first month of soil growth at 10 °C (Fig. 3A and Supplemental Fig. S3A). It continued to produce new leaves and slow growth after 3 mo at 10 °C when the *aca8 aca10* mutant died at that point (Supplemental Fig. S3B). However, the *aca8 aca10 fmo1* mutant continued in the vegetative stage without dying, while the wild-type plants set seeds

at after 5 mo 10 °C. Therefore, the *fmo1* mutation that significantly reduces defense responses partially rescued chilling susceptibility in the *aca8 aca10* mutant, suggesting that *ACA8* and *ACA10* affect chilling tolerance at least partially through their effect on plant defense responses.

Low $[Ca^{2+}]_{ext}$ reduces autoimmunity and rescues chilling lethality in the *aca8 aca10* mutant

Since low $[Ca^{2+}]_{ext}$ reduced resting $[Ca^{2+}]_{cyt}$ and reduced defense responses in *aca8 aca10*, we tested whether or not the low $[Ca^{2+}]_{ext}$ could rescue the chilling-susceptible phenotype of *aca8 aca10*. Similar to the soil-grown plants, the hydroponically grown *aca8 aca10* plants were reduced in rosette size compared to the wild type at 10 °C and 22 °C irrespective of $[Ca^{2+}]_{ext}$ (Supplemental Fig. S3, C–E). The *aca8 aca10* plants grown under 0.1 mM $[Ca^{2+}]_{ext}$ in general had larger and greener rosettes compared to those grown under 1.5 mM $[Ca^{2+}]_{ext}$ at 10 °C (Fig. 3B and Supplemental Fig. S3D). Quantification of rosettes showed that the *aca8 aca10* had a higher fresh weight at 0.1 mM $[Ca^{2+}]_{ext}$ than at 1.5 mM $[Ca^{2+}]_{ext}$ at 10 °C (Fig. 3C), supporting that a lower $[Ca^{2+}]_{ext}$ partially rescued the chilling susceptibility of the *aca8 aca10* mutant.

To further investigate whether defense response activation was responsible for chilling susceptibility in the *aca8 aca10* mutant, we analyzed the expression of the above-mentioned 23 defense-related genes that were upregulated in the *aca8 aca10* at 22 °C (Fig. 2C). Heatmap was used to visualize expression patterns of this set of genes in wild type and the *aca8 aca10* mutant growth under 0.1 and 1.5 mM $[Ca^{2+}]_{ext}$ with or without the 10 °C chilling growth of 21 d (Fig. 3D). Chilling moderately increased the expression of these genes at 0.1 and at 1.5 mM $[Ca^{2+}]_{ext}$ in the wild type, and it drastically increased their expression in the *aca8 aca10* mutant (Fig. 3D, Supplemental Data Set S2). Importantly, expressions of the majority of these genes (21 out of 23) were higher at high $[Ca^{2+}]_{ext}$ compared to low $[Ca^{2+}]_{ext}$ in *aca8 aca10* under chilling. For instance, the expression of the SA biosynthesis gene *SID2* had the lowest expression in the wild type grown at 22 °C under 0.1 mM $[Ca^{2+}]_{ext}$ and the highest expression in the *aca8 aca10* mutant at 10 °C under 1.5 mM $[Ca^{2+}]_{ext}$ (Supplemental Fig. S3F). Its expression under chilling was significantly lower at 0.1 mM $[Ca^{2+}]_{ext}$ than at 1.5 mM $[Ca^{2+}]_{ext}$. Similarly, the expression of *CBP60g* was highest in the mutant grown at 10 °C under 1.5 mM $[Ca^{2+}]_{ext}$ but significantly reduced when grown under 0.1 mM $[Ca^{2+}]_{ext}$ (Supplemental Fig. S3G). These expression changes indicate that autoimmunity was further enhanced in the *aca8 aca10* mutant under chilling and these changes were associated with an elevated $[Ca^{2+}]_{cyt}$.

Interestingly, a slightly elevated resting $[Ca^{2+}]_{cyt}$ (indicated by the YC3.6 reporter) was observed in guard cells after plants were grown at 10 °C for 5 d compared to at 22 °C (Fig. 3E). This is associated with a higher expression of defense-related genes at low temperature in the wild type.

The *aca4 aca11* mutant exhibits autoimmunity and chilling susceptibility associated with an elevated resting $[Ca^{2+}]_{cyt}$ level

The mutant of vacuole-localized ACA4 and ACA11, *aca4a ca11*, was shown to have an elevated resting $[Ca^{2+}]_{cyt}$ compared to the wild type (Hilleary et al. 2020), similar to *aca8 aca10*. We hypothesized that this high resting $[Ca^{2+}]_{cyt}$ is responsible for the autoimmunity observed in the *aca4 aca11* mutant and that the *aca4 aca11* mutant would have a chilling-susceptible phenotype similar to the *aca8 aca10* mutant. To test this hypothesis, we grew seedlings of the wild-type and *aca4 aca11 sid2* mutant hydroponically in a medium with $[Ca^{2+}]_{ext}$ at 0.1 or 1.5 mM. The *sid2* mutation greatly suppressed cell death and autoimmunity in *aca4 aca11* (Boursiac et al. 2010), which would remove or greatly reduce potential indirect effects of autoimmunity on $[Ca^{2+}]_{cyt}$. The resting $[Ca^{2+}]_{cyt}$ in *aca4 aca11 sid2* was found to be significantly reduced under lower $[Ca^{2+}]_{ext}$ compared to under 1.5 mM $[Ca^{2+}]_{ext}$ based on the reporter mCherry-GCaMP6f (Fig. 4A). The *aca4 aca11* mutant exhibited cell death on leaves when grown under 1.5 mM $[Ca^{2+}]_{ext}$, but cell death was greatly reduced when plants were grown under 0.1 mM $[Ca^{2+}]_{ext}$ (Fig. 4B). This indicates that the cell death defect is likely caused by an elevated resting $[Ca^{2+}]_{cyt}$ in *aca4 aca11*. In addition, the growth of *Pst* DC3000 was analyzed in *aca4 aca11* grown under 0.1 or 1.5 mM $[Ca^{2+}]_{ext}$. While pathogen growth was lower by 10-fold in the *aca4 aca11* mutant compared to the wild type under 1.5 mM $[Ca^{2+}]_{ext}$, it grew to a similar extent in the wild type and the mutant under 0.1 mM $[Ca^{2+}]_{ext}$ (Fig. 4C). This indicates that a high resting $[Ca^{2+}]_{cyt}$ likely contributes to enhanced defense response in *aca4 aca11*, in addition to *aca8 aca10*.

Tolerances to chilling were further analyzed for the *aca4 aca11* mutant. Similar to the *aca8 aca10* mutant, the *aca4 aca11* mutant plants also died after 1 month's growth at 10 °C, whereas the wild-type plants were all alive (Fig. 4D). Consistent with the hypothesis that chilling susceptibility is induced by autoimmunity, and the *aca4 aca11 sid2* plants, where SA biosynthesis is reduced, survived the chilling treatment (Fig. 4D). Furthermore, a lower $[Ca^{2+}]_{ext}$ rescued the chilling lethality phenotype of the *aca4 aca11* plants. While the *aca4 aca11* plants were all dead after 4 wk at 10 °C when hydroponically grown under 1.5 mM $[Ca^{2+}]_{ext}$, they all survived when grown under 0.1 mM $[Ca^{2+}]_{ext}$ (Fig. 4E).

ACA10 and *ACA8* are critical for plant survival at high temperatures

To determine the roles of *ACA8* and *ACA10* in heat tolerance, we subjected the *aca8 aca10* mutant plants to heat stresses. Seedlings of the mutant and the wild type were first grown at 22 °C for 2 wk and then grown at 35 °C. No apparent morphological difference was observed between the *aca8 aca10* mutant and the wild type in the first week at 35 °C, but the mutant became yellower compared to the wild type

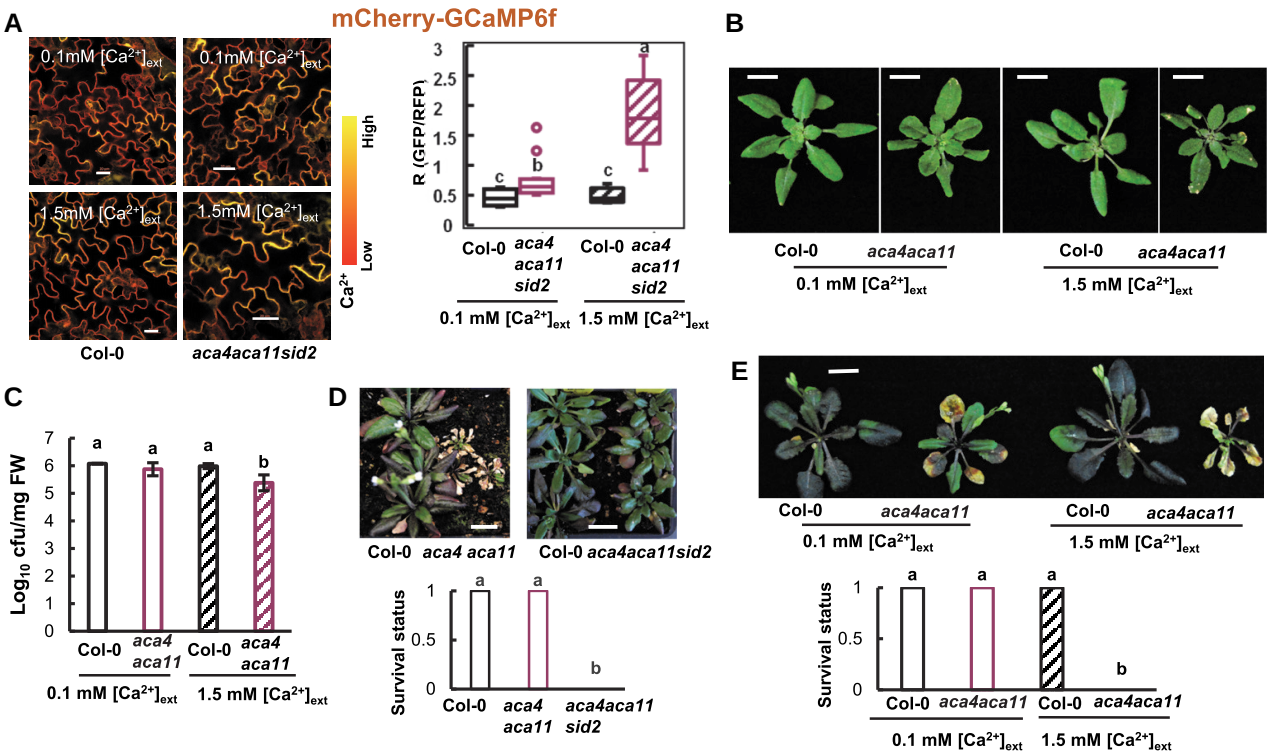

Figure 4. The *aca4 aca11* mutant has a reduced autoimmunity under low $[Ca^{2+}]_{ext}$ and is more chilling susceptible compared to the wild type. A) Images and quantification (in box plot) of fluorescence signal ratios of GFP/RFP from the reporter mCherry-GCaMP6f in leaf epidermal cells of the wild-type Col-0 and the *aca4 aca11sid2* mutant plants containing the reporter grown hydroponically at 0.1 or 1.5 mM $[Ca^{2+}]_{ext}$. The scale bar is 20 μm. More than 10 cells (1 cell/plant) for each genotype were measured for quantification. Different letters indicate statistically significant differences tested by ANOVA ($P < 0.05$). For the box-whisker plot, the top and bottom sides of the box are the upper and lower quartiles; the line in the box is the median; the whiskers mark the range from maximum to minimum or 1.5 times the interquartile range with outliers represented as a circle. B) Phenotypes of wild-type Col-0 and *aca4 aca11* plants grown hydroponically at 0.1 or 1.5 mM $[Ca^{2+}]_{ext}$ for 21 d. C) Growth of *Pst* DC3000 in wild-type Col-0 and *aca4 aca11* seedlings hydroponically grown under 0.1 and 1.5 mM $[Ca^{2+}]_{ext}$. Seedlings were grown under a 12/12-h photoperiod at 22 °C for 14 d before they were infected with *Pst* DC3000. Shown are mean values and SD (standard deviation) of log_{10} value of the bacterial number (cfu per mg FW) in leaves at 3 d after infection from 3 biological repeats in one representative experiment. Similar results were obtained from 2 independent experiments (each with 3 biological repeats). Different letters indicate statistically significant differences tested by ANOVA ($P < 0.05$). D) Phenotype and survival status of wild-type Col-0, *aca4 aca11*, and *aca4 aca11 sid2* grown at 10 °C (following 5 d of germination and growth at 22 °C). Plant images were taken at 1 mo's growth at 10 °C, and the survival status (1 as live and 0 as dead) was analyzed at 3 mo' growth at 10 °C. More than 27 plants were analyzed for each genotype. Different letters indicate statistically significant differences tested by ANOVA ($P < 0.05$). E) Phenotypes and survival status of wild-type Col-0 and *aca4 aca11* plants grown hydroponically under 0.1 and 1.5 mM $[Ca^{2+}]_{ext}$ at 22 °C for 14 d and then 10 °C for 28 d. More than 22 plants for each genotype were analyzed. Different letters indicate statistically significant differences tested by ANOVA ($P < 0.05$).

afterward and the difference became more drastic as heat treatment continued. After 4 wk at 35 °C, the *aca8 aca10* mutant plants were all dead, whereas the wild-type plants were all alive (Fig. 5A). This shows that the *ACA8* and *ACA10* are essential for plant survival at high temperatures. High temperature is known to inhibit SA-mediated immune responses (Hua 2013), and we expected that this heat tolerance defect in the *aca8 aca10* mutant was not due to autoimmunity, unlike that of the chilling tolerance defect. This was verified by the investigation of heat tolerance of the *aca8 aca10 fmo1* mutant where autoimmunity was largely suppressed. The *fmo1* mutation did not significantly alter heat tolerance, and the *fmo1* mutant was alive after 4 wk at 35 °C, similarly to the wild type (Fig. 5A). The *aca8 aca10 fmo1* mutant, like *aca8 aca10*, died after 4 wk at 35 °C (Fig. 5A). A similar heat susceptibility was also observed for the *aca8 aca10* mutant at 42 °C. After 10 d of 42 °C treatment of 2-wk-old seedlings, the *aca8 aca10* and *aca8 aca10 fmo1* plants were dead but the wild type Col-0 and *fmo1* plants were alive (Supplemental Fig. S4A). This indicates that *ACA8* and *ACA10* regulate heat tolerance independent of their defense regulation. Similar to the *aca8 aca10* mutant, the *aca4 aca11* mutant plants all died, whereas the wild-type plants were all alive after 4 wk of heat treatment at 35 °C or 11 d of heat treatment at 42 °C (Fig. 5B and Supplemental Fig. S4B).

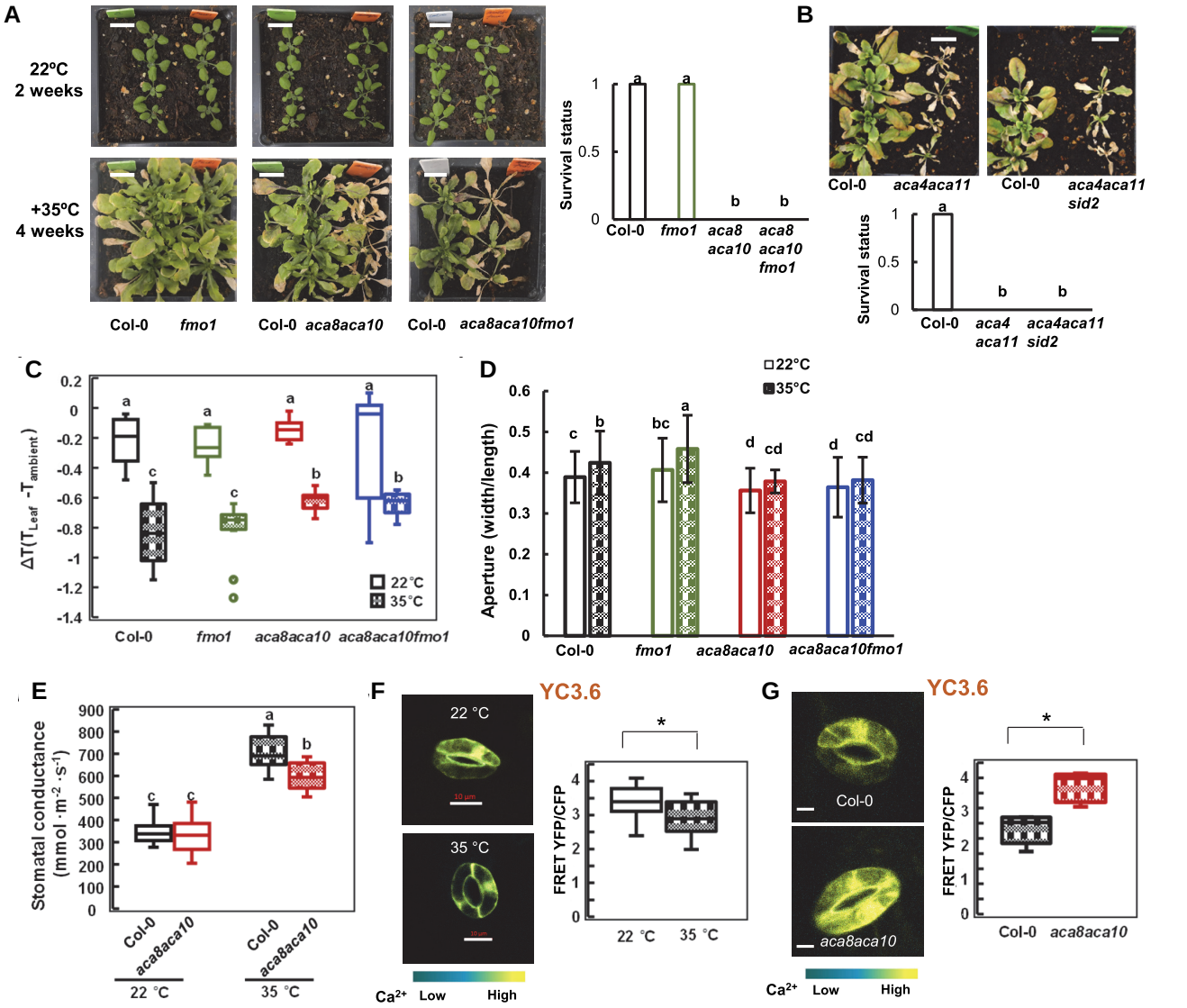

Figure 5. Heat susceptibility of the *aca8 aca10* mutant is associated with high $[Ca^{2+}]_{cyt}$, high leaf temperature, and high HSP expression. Growth phenotypes and survival status of wild-type Col-0, *fmo1*, *aca8 aca10*, and *aca8 aca10 fmo1* plants A) or Col-0 and the *aca4 aca11* mutant plants B) under heat. Seedlings were grown at 22 °C for 2 wk and then at 35 °C for 4 wk before being photographed (scale bar, 10 mm). More than 34 plants A) or 22 plants B) for each genotype were analyzed for survival status (1 for live and 0 for dead). Different letters indicate significant differences among samples by ANOVA test ($P < 0.05$). C) Leaf temperature expressed as ΔT (difference between leaf and ambient temperatures) of wild-type Col-0, *fmo1*, *aca8 aca10*, and *aca8 aca10 fmo1* at 22 °C and 35 °C. Plants were grown at 22 °C for 21 d and were then moved to 35 °C for 1 d. Shown are mean values ± SD from measurements of 10 leaves each from a different plant. T_{leaf}, leaf temperature; $T_{ambient}$, ambient temperature. Different letters indicate significant differences among samples by ANOVA test ($P < 0.05$). D) Stomatal apertures (expressed as width/length of the pore) of wild-type Col-0 and *aca8 aca10* at 22 °C and 35 °C. Shown are mean values ± SD from 35 stomata. Plants were grown at 22 °C and moved to 35 °C for 1 d (same as in C). Epidermis layers were peeled, floated on ddH_2O, and observed under a microscope, all done under the respective temperatures. Different letters indicate significant differences among samples by ANOVA test ($P < 0.05$). E) Stomatal conductance of wild-type Col-0 and *aca8 aca10* at 22 °C and 35 °C. Shown are mean values ± SD from measurements of 12 leaves each from a different plant. Plants were grown at 22 °C and moved to 35 °C for 1 d (same as in C). Different letters indicate significant differences among samples by ANOVA ($P < 0.05$). Images and quantification of $[Ca^{2+}]_{cyt}$ signal shown as FRET-YFP and CFP ratio from YC3.6 in guard cells of 3-wk-old wild-type Col-0 plants grown at 22 °C or 35 °C for additional 5 d F) or 3-wk-old plants of wild-type Col-0 and *aca8 aca10* grown at 35 °C for 5 d G). The scale bar is 10 μm. Data were obtained from more than 10 stomata (each from a different leaf) for each genotype. "*" indicates a statistically significant difference between samples determined by Student's *t*-test (*$P < 0.05$). For box-whisker plots in C), E), F), and G), the top and bottom sides of the box are the upper and lower quartiles; the line in the box is the median; the whiskers mark the range from maximum to minimum or 1.5 times the interquartile range with outliers represented as a circle.

The *aca8 aca10* mutant is more susceptible to heat and has a higher leaf temperature under heat than the wild type

To reveal how *ACA8* and *ACA10* regulate heat tolerance in Arabidopsis, we carried out a transcriptome analysis on the wild-type Col-0, *fmo1*, *aca8 aca10*, and *aca8 aca10 fmo1* plants under heat treatment. Plants were grown at 22 °C for 2 wk before they were heat treated at 42 °C, and RNAs were extracted from leaf tissues at 0 d (before treatment), 1 d, and 7 d. Cluster analysis of DEGs revealed 5 major groups for these 4 genotypes at 3 time points (Supplemental Fig. S5A). Genes in group 1 had expression patterns associated with the heat-susceptible phenotype among the 4 genotypes: they were highest in *aca8 aca10* and *aca8 aca10 fmo1* compared to the wild type and the *fmo1* mutant at 7 d at 42 °C (Supplemental Fig. S5A). GO analysis of these DEGs revealed an enrichment of the terms related to heat response such as "response to hydrogen peroxide," "cellular response to heat," "heat response," and "heat acclimation" (Supplemental Fig. S5B). More specifically, heat stress transcription factor (HSF) genes and heat shock protein (HSP) genes are shared under these terms. Expressions of 6 HSF and 15 HSP genes were induced by 1 d of 42 °C in the wild type and the *fmo1* mutant, and the induction was higher in *aca8 aca10* and *aca8 aca10 fmo1* compared to the wild type or *fmo1* (Supplemental Fig. S5C). The difference became more drastic at 7 d of 42 °C treatment with expression of *HSP*s and *HSF*s at 1.5- to 10-fold higher in *aca8 aca10* and *aca8 aca10 fmo1* compared to in wild-type Col-0 and *fmo1* (Supplemental Fig. S5C, Supplemental Data Set S3). For instance, expression of *HSP22* was 2-fold higher in the *aca8 aca10* mutant at 1 d of 42 °C but was increased to 6-fold at 7 d of 42 °C compared to the wild-type Col-0 (Supplemental Fig. S5D). The expression of *HSP70* was increased to a comparable high level in the mutant and the wild type at 1 d of 42 °C, and it further increased in the *aca8 aca10* mutant but not as much in the wild type at 7 d of 42 °C treatment (Supplemental Fig. S5D). This suggests that the *aca8 aca10* mutant may experience a more severe heat stress than wild-type Col-0 under the same heat conditions. Corroborated with this hypothesis, another term "long-chain fatty acid metabolic process" enriched for DEGs of *aca8 aca10* at 42 °C was associated with heat stress (De Bigault and Cacas 2016), suggesting a higher heat stress in the mutant.

We explored the possibility that the mutant was experiencing a higher leaf temperature than the wild type under the same heat condition. To this end, leaf surface temperatures were measured by the photosynq MultispeQ on 3-wk-old plants of wild-type Col-0, *fmo1*, *aca8 aca10*, and *aca8 aca10 fmo1* that were treated by 35 °C for 1 d. The difference between temperatures of leaf and ambient air (ΔT) that were measured simultaneously was used to reflect the leaf surface temperature. At 22 °C, ΔTs of *aca8 aca10* and *aca8 aca10 fmo1* were not significantly different from those of the wild-type Col-0 and *fmo1* (Fig. 5C). However, at 35 °C, ΔTs of *aca8 aca10* and *aca8 aca10 fmo1* were significantly higher than those of the wild-type Col-0 and *fmo1* (Fig. 5C). This indicates that *ACA8* and *ACA10* affect leaf surface temperatures under heat.

The *aca8 aca10* mutant has less opened stomata and less transpiration under heat compared to the wild type

Previous study showed that *ACA8* and *ACA10* regulate stomatal aperture. The stomata of the *aca8 aca10* mutant were more closed than the wild type at 22 °C, and they did not close in response to pathogen, external Ca^{2+}, or ABA (Yang et al. 2017; Yu et al. 2018). We, therefore, examined the stomatal aperture of the *aca8 aca10* mutants at 35 °C. Consistent with the previous findings, stomata were more closed in *aca8 aca10* than in wild-type Col-0 at 22 °C, and there was no significant difference in stomatal aperture between *aca8 aca10 fmo1* and *aca8 aca10* (Fig. 5D). The wild type had more opened stomata at 35 °C compared to 22 °C, suggesting an increased transpiration under heat to lower leaf temperature. The *aca8 aca10* and *aca8 aca10 fmo1* mutants did not open stomata significantly in response to heat and had more closed stomata compared to the wild-type Col-0 or *fmo1* at 35 °C. This indicates that *ACA8* and *ACA10* negatively regulate stomatal closure at both 22 °C and 35 °C.

We subsequently measured the stomatal conductance to determine if lethality in *aca8 aca10* might result from low transpiration. The wild type had a higher stomatal conductance at 35 °C compared to 22 °C (Fig. 5E), indicating a higher transpiration to facilitate leaf cooling. The *aca8 aca10* mutant also had a higher stomatal conductance at 35 °C compared to at 22 °C, but it had a lower conductance at 35 °C compared to the wild type (Fig. 5E). This likely contributes to the higher leaf temperature and lethality of the *aca8 aca10* mutant at high temperatures.

Because calcium signals have been implicated in controlling stomatal apertures (Kudla et al. 2010), we examined $[Ca^{2+}]_{cyt}$ level in guard cells of the *aca8 aca10* mutant and the wild-type Col-0 at 35 °C. The $[Ca^{2+}]_{cyt}$ was higher in *aca8 aca10* than in Col-0 at 35 °C (Fig. 5G), similarly to 22 °C. Interestingly, the $[Ca^{2+}]_{cyt}$ was lower at 35 °C compared to 22 °C in the wild type (Fig. 5F). This suggests that more closed stomata in *aca8 aca10* could result from the elevated $[Ca^{2+}]_{cyt}$ in the *aca8 aca10* mutant.

Basal and peak levels of transient Ca^{2+} signals triggered by flg22, cold, and heat are elevated in the *aca8 aca10* mutant

ACA8 and ACA10 maintain low resting $[Ca^{2+}]_{cyt}$ and prevent activation of defense response genes before pathogen infection, and the upregulation of defense response genes prior to infection could account for reduced pathogen growth (enhanced resistance) observed in the *aca8 aca10* mutant. Similarly, the *aca8 aca10* defects in tolerance to long-term

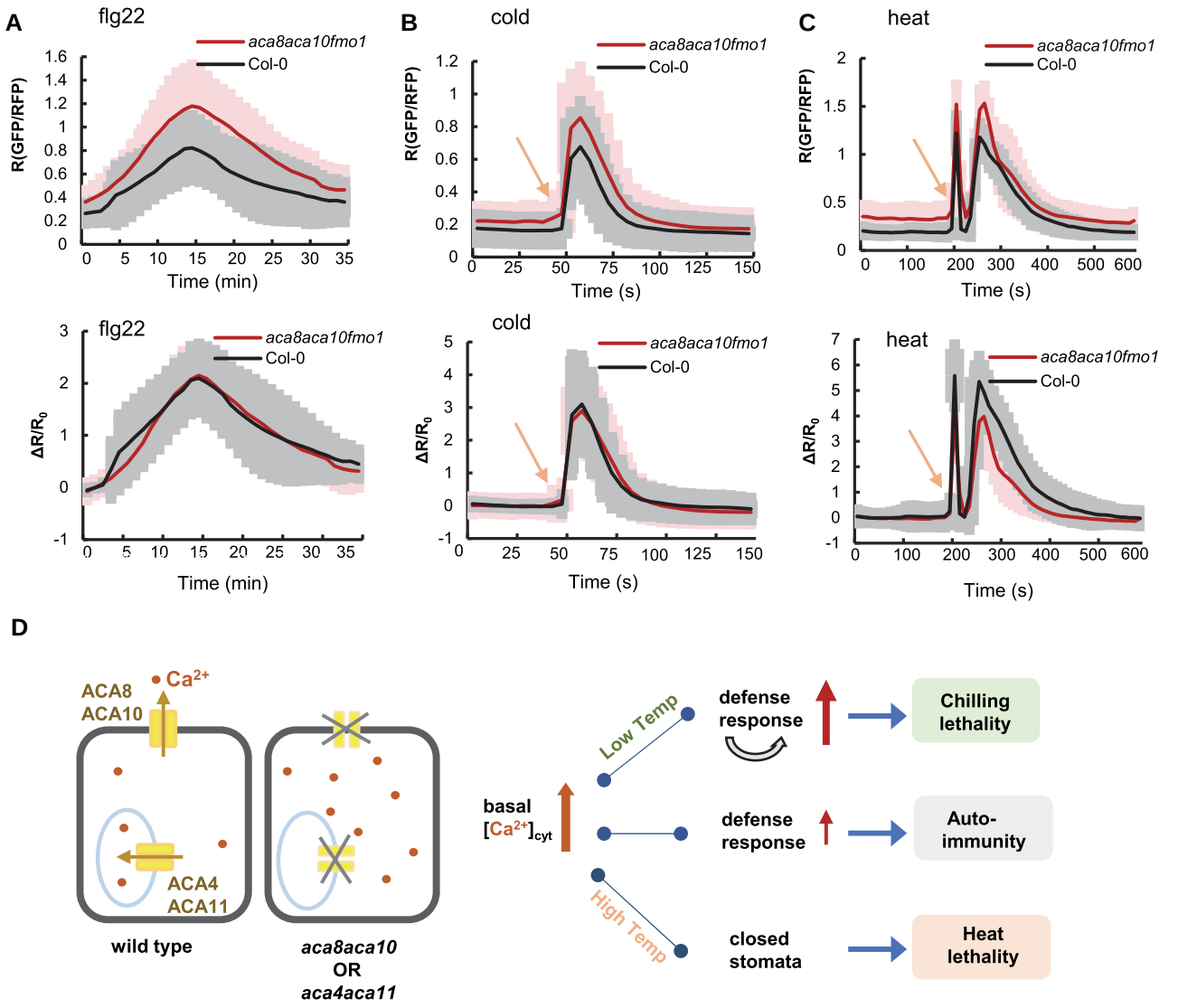

Figure 6. $[Ca^{2+}]_{cyt}$ response to elicitor, cold, and heat in the *aca8 aca10* mutant. $[Ca^{2+}]_{cyt}$ responses to flg22 A), cold B), and heat C) in epidermal cells of wild-type Col-0 and *aca8 aca10 fmo1* mutant measured by the mCherry-GCaMP6f reporter. Shown are averages and SD (error bars) of the GFP/RFP ratio (upper panel) and fractional ratio changes $\Delta R/R_0$ (lower panel). In A), signals in response to 200 nM flg22 were captured every minute, and signals from 15 min before the peak to 20 min after the peak from a total of 8 cells (1 cell/plant) for each genotype are aligned at the peak. For B), leaves were taped on slides, and ice water was added to a slide as cold treatment. Arrow indicates the time of cold application. Data were from a total of 12 cells (1 cell/plant) for each genotype. For C), leaves were taped on slides, and heat treatment was applied by adding water of 42 °C to slides. Arrow indicates the time of heat application. Data are from 10 cells (1 cell/plant) for each genotype. D) Model of calmodulin-regulated Ca^{2+} pumps function. The primary functions of PM-localized Ca^{2+} pumps ACA8 and ACA10 as well as the vacuole-localized pumps ACA4 and ACA11 are to maintain low resting $[Ca^{2+}]_{cyt}$, and the resting level of $[Ca^{2+}]_{cyt}$ has a large impact on biotic and abiotic stress responses. Elevated resting $[Ca^{2+}]_{cyt}$ in the *aca8 aca10* or *aca4 aca11* mutants causes autoimmunity with mis-regulated expression of defense response genes. Under chilling, this autoimmunity is amplified leading to cell death and chilling susceptibility. Under heat, elevated resting $[Ca^{2+}]_{cyt}$ induces closed stomata and heat susceptibility.

treatment of cold and heat can also be accounted by elevated resting $[Ca^{2+}]_{cyt}$ level. We further asked whether or not ACA8 and ACA10 have an additional role in regulating transient $[Ca^{2+}]_{cyt}$ in response to environmental stimuli.

Using the ratiometric calcium reporter mCherry-GCaMP6f, we compared transient Ca^{2+} signal in responses to the elicitor flg22 peptide, cold, and heat in epidermal cells of the wild-type Col-0 and the *aca8 aca10 fmo1* mutant where autoimmunity is blocked. After the flg22 application, the wild-type Col-0 and the *aca8 aca10* mutant had a similar response dynamic in $[Ca^{2+}]_{cyt}$ elevating, peaking, and decreasing (Supplemental Movies S1 and S2). The *aca8 aca10* mutant had higher peak and basal $[Ca^{2+}]_{cyt}$ levels as measured by R (ratio) of GFP/RFP compared to the wild type (Fig. 6A). We further analyzed Ca^{2+} response to flg22 by fractional ratio changes ($\Delta R/R_0$) to remove the effect of basal $[Ca^{2+}]_{cyt}$. The response measured

by $\Delta R/R_0$ was similar in the *aca8 aca10* and wild-type Col-0 (Fig. 6A).

After cold treatment, a $[Ca^{2+}]_{cyt}$ increase was initiated quickly with a peak at 10 s after treatment in the wild type (Fig. 6B, Supplemental Movies S3 and S4), similar to earlier reports (Knight and Trewavas 1996 ; Cui et al. 2020). A transient $[Ca^{2+}]_{cyt}$ response to cold was initiated at the same time in the *aca8 aca10 fmo1* mutant (Fig. 6B). The peak level was higher in the mutant compared to wild type, but the Ca^{2+} response was similar between the wild type and the mutant as indicated by $\Delta R/R_0$ (Fig. 6B). After heat treatment, the wild type had a first $[Ca^{2+}]_{cyt}$ spike that peaked at 10 s and a second $[Ca^{2+}]_{cyt}$ spike that peaked at 60 s (Fig. 6C, Supplemental Movies S5 and S6). A similar dynamic of the transient calcium response to heat was observed in the *aca8 aca10 fmo1* mutant, and the basal levels and peak levels of $[Ca^{2+}]_{cyt}$ were higher in the mutant compared to the wild type (Fig. 6C). The $[Ca^{2+}]_{cyt}$ response dynamics measured by $\Delta R/R_0$ was similar in the first peak but was lower (but not statistically different) for the second peak in the *aca8 aca10* compared to the wild-type Col-0 (Fig. 6C).

Discussion

Ca^{2+} transporting systems are thought to play essential roles in maintaining Ca^{2+} homeostasis and generating Ca^{2+} signals that are important for plant growth, development, and environmental responses. Here, we investigated the function of 2 major PM-localized ACA-type Ca^{2+} pumps, ACA8 and ACA10, as well as 2 vacuole-localized pumps, ACA4 and ACA11, in regulating cytosolic Ca^{2+} signals and environmental responses. A loss of their function resulted in plants with multiple defects, including an autoimmune response with a reprogrammed transcriptome and hyper-susceptibility to chilling or heat. Using 3 different Ca^{2+} reporters, GCaMP6s, YC3.6, and mCherry-GCaMP6f, we observed elevated resting $[Ca^{2+}]_{cyt}$ in both leaf epidermal pavement cells and guard cells in the *aca8 aca10* mutant compared to the wild-type Col-0 (Fig. 1, A and B). These abnormal resting levels of $[Ca^{2+}]_{cyt}$ were initially observed in plants grown under standard conditions in either soil or hydroponics with 1.5 mM $[Ca^{2+}]_{ext}$. However, a restoration of near-normal resting $[Ca^{2+}]_{cyt}$ levels was achieved using hydroponics in which $[Ca^{2+}]_{ext}$ was reduced by more than 10-fold from 1.5 to 0.1 mM. This reduction in external Ca^{2+} also suppressed the *aca8 aca10-* and *aca4 aca11*-dependent phenotypes associated with chilling and autoimmunity noted above (including changes in the transcriptome, see Fig. 2C). The effects of reduced $[Ca^{2+}]_{ext}$ on heat susceptibility were not determined due to difficulty in setting up long-term hydroponic growth under heat. Nevertheless, this suppression of autoimmunity and chilling sensitivity provides strong evidence that at least some of the most observable phenotypes were caused by (or exacerbated by) elevations in the basal resting $[Ca^{2+}]_{cyt}$.

Similar elevations in resting $[Ca^{2+}]_{cyt}$ levels were previously reported in plants harboring a knockout of the vacuole-localized ACAs (*aca4 aca11*) as well as the ER-localized ACAs, *aca1 aca2 aca7* (Hilleary et al. 2020; Rahmati Ishka et al. 2021). This was confirmed here for *aca4 aca11* using the ratiometric reporter mCherry-GCaMP6f, a Ca^{2+} reporter fused with mCherry in order to normalize Ca^{2+} signals between different plants, plant tissues, or conditions. It is noted that while all these LOF mutants have elevated resting $[Ca^{2+}]_{cyt}$ in leaves, the *aca8 aca10* and *aca4 aca11* mutants were reported to have wild-type level of $[Ca^{2+}]_{cyt}$ in roots (Costa et al. 2017; Hilleary et al. 2020). This suggests some tissue-specific variation in how different efflux systems contribute to maintaining $[Ca^{2+}]_{cyt}$ levels.

These combined results indicate that different subsets of ACA pumps on multiple membranes can all make significant contributions to the maintenance of low resting $[Ca^{2+}]_{cyt}$. Given that the 3 sets of *aca* knockouts (PM, *aca8 aca10*; Vacuole, *aca4 aca11*; *and* ER, *aca1 aca2 aca7)* all display leaves with some degree of enhanced autoimmunity, this raises a question of whether elevated resting $[Ca^{2+}]_{cyt}$ in these mutants might arise from an indirect consequence of an autoimmunity-triggered Ca^{2+} influx into the cytosol (Bi et al. 2021; Jacob et al. 2021). Despite this concern, genetic evidence here indicates that elevated resting $[Ca^{2+}]_{cyt}$ in the *aca8 aca10* mutant remained high even after the suppression of the autoimmunity phenotype with an *fmo1* knockout mutation that abolishes NHP biosynthesis and inhibits SA signaling (Fig. 1, A and C). Similarly for an *aca4 aca11* mutant, resting $[Ca^{2+}]_{cyt}$ remained elevated even after the suppression of the autoimmunity phenotype with a *sid2* mutation. Both *FMO1* and *SID2* are important for SA-dependent systemic-acquired immunity, and mutations in these genes block immune responses to a great extent (Wildermuth et al. 2001; Hartmann et al. 2018). Thus, the failure of *fmo1* or *sid2* to restore normal resting $[Ca^{2+}]_{cyt}$ in *aca8 aca10* or *aca4 aca11* indicates that the observed elevations in resting levels are not an indirect effect of autoimmunity. While it is not yet clear how autoimmunity is triggered, or the specific role of Ca^{2+} in its systemic propagation, results here highlight the importance of high-affinity Ca^{2+} pumps in maintaining low resting $[Ca^{2+}]_{cyt}$ levels to prevent an inappropriate activation of pathogen defense responses.

In addition to setting cytosolic resting levels of $[Ca^{2+}]_{cyt}$, ACA8 and ACA10 also have an effect on transient signal. Mutant plants harboring *aca8 aca10* LOF mutations displayed transient Ca^{2+} signals with increased peak levels in response to a pathogen elicitor, chilling, and heat stress (Fig. 6, A–D; Supplemental Movies S1–S6). Although there is an increase of absolute peak level in the mutant compared to the wild type, the relative increase of $[Ca^{2+}]_{cyt}$ level over the basal $[Ca^{2+}]_{cyt}$ level, as indicated by $\Delta R/R_0$, was not substantially different between the *aca8 aca10* mutant and the wild type (Fig. 6, A–C). As these transient responses have high variability, future studies with a larger sample number might determine if there are small differences in relative $[Ca^{2+}]_{cyt}$ response to flg22, heat, and cold caused by the loss of ACA8 and ACA10 in addition to basal $[Ca^{2+}]_{cyt}$. An increase

of $[Ca^{2+}]_{cyt}$ response was observed for a wounding signal in an *aca8* mutant (Costa et al. 2017) and for an flg22-triggered signal in *aca4 aca11* and *aca1 aca2 aca7* mutants (Hilleary et al. 2020; Rahmati Ishka et al. 2021), whereas a decrease of $[Ca^{2+}]_{cyt}$ response was observed for ATP stimulus in the *aca8 aca10* mutant (37). Future studies should reveal whether the loss of ACA-type pumps at different locations might differentially affect the relative magnitudes of Ca^{2+} signals in a trigger-specific manner, and if so, whether or not the resting Ca^{2+} level contributes to the amplitude of transient signal. More extensive analysis of transient signals to multiple stimuli under different $[Ca^{2+}]_{ext}$ levels could be investigated in the future to probe the potential connection between the peak magnitudes and basal starting points that are set by the calcium pumps.

This study reveals a critical role in cold stress tolerance for both the PM-localized ACA8 and ACA10 and vacuole-localized ACA4 and ACA11. Their LOF accelerates cell death and lethality at 10 °C. Interestingly, this chilling lethality is prevented by suppressing autoimmunity with the *fmo1* mutation in *aca8 aca10* (Fig. 3A and Supplemental Fig. S4B), or the *sid2* mutation for *aca4 aca11*. Autoimmunity in the *aca8 aca10* mutant is more pronounced at low temperature compared to normal temperature (Fig. 3D). This is consistent with the early findings that low temperature enhances SA biosynthesis and NLR protein activity and that NLR could form an amplification loop with SA to enhance resistance at low temperature (Li et al. 2019). Autoimmunity with up-regulation of the SA/NLR pathway induces plant cell death and hybrid necrosis which are enhanced by low temperature (Bomblies et al. 2007; Wang et al. 2013). These results emphasize the contribution of biotic stress response to low-temperature responses in Arabidopsis.

This study also revealed a critical role in heat stress tolerance for both ACA8/ACA10 and ACA4/ACA11. Their LOF accelerates cell death and lethality at 35 °C (Fig. 5, A and C; Supplemental Fig. S5). However, in contrast to the cold stress response, this hypersensitivity was not prevented by suppressing the autoimmunity phenotype with *fmo1* or *sid2*, which is consistent with the early finding of high-temperature suppression of SA-mediated immune responses (Hua 2013). Gene expression studies suggest that this heat susceptibility does not result from a deficient short-term heat shock response, as heat shock response genes were induced by heat in both the *aca8 aca10* mutant and the wild type (Supplemental Fig. S5C). However, the mutant showed a higher leaf surface temperature, which was associated with the observation that stomatal apertures were more closed, which would reduce the cooling potential from evapotranspiration (Fig. 5, C–E). This supports a model in which an elevation in resting $[Ca^{2+}]_{cyt}$ could impact stomatal aperture regulation and thereby make *aca8 aca10* and *aca4 aca11* mutants hypersensitive to heat stress.

In sum, we show here that PM and endomembrane ACAs all make significant contributions to maintaining a low resting $[Ca^{2+}]_{cyt}$, and that an elevation in the resting level of $[Ca^{2+}]_{cyt}$ has a different impact on biotic and abiotic stress responses (Fig. 6D). However, additional studies are needed to define potential tissue-specific and location-specific functions for different subsets of pumps that are localized to the PM, ER, and vacuole. In addition, it is not yet clear what additional unique or shared contributions are provided by other calcium efflux systems, such as ECAs and calcium-exchangers (CAXs) (Shigaki and Hirschi 2006; Garcia Bossi et al. 2020). Regardless, the results here establish the importance of ACA-type Ca^{2+} pumps in maintaining a low resting $[Ca^{2+}]_{cyt}$ that prevents autoimmune responses and impact a plant's tolerance to hot and cold temperatures.

Materials and methods

Plants growth conditions

The Arabidopsis (*Arabidopsis thaliana*) plants were grown in chambers with a light intensity of 70 to 100 µmol m^{-2} s^{-1} and a relative humidity of 50% to 70%. Plants were grown under constant light unless they were used for pathogen growth assay where they were grown under a 12-h light/12-h dark photoperiod.

The hydroponic culture was performed as previously described with slight modification (Tian et al. 2019). Arabidopsis seeds were sown on plates on half-strength Murashige and Skoog solid medium with 1% (w/v) sucrose and 7 g L^{-1} agar. After 2 d of 4 °C treatment in the dark, seeds were germinated under constant light at 22 °C. Five-day-old seedlings were transferred onto a floating foam support and placed in a 300-ml box covered by foil and filled with a standard hydroponic solution of 0.2 mM KH_2PO_4, 3 mM KNO_3, 1 mM NH_4NO_3, 0.25 mM $MgSO_4$, 0.01632 g L^{-1} micronutrient (Caisson Labs), and 0.1 or 1.5 mM $CaCl_2$ (pH 5.8, adjusted with NaOH). The hydroponic solutions were replaced by fresh solutions every week.

Generation of transgenic plants

The GCaMP6s cassette was amplified from HBT-GCaMP6-HA (Liu et al. 2017) by PCR and cloned into $PCR8^{gw}$ vector and then cloned into the binary vector pMDC99 by LR reaction of the Gateway system (Curtis and Grossniklaus 2003). The construct was transformed into *Agrobacterium* and then Arabidopsis plants via floral dipping. Primers used for generating constructs and genotyping are provided in Supplemental Data Set S4.

EMS mutagenesis and cloning of the suppressor gene

Approximately 7,000 seeds were treated with 0.25% EMS for 12 h with gentle shaking. Ten M1 plants were pooled for collecting M2 seeds. Approximately 100 seeds from each pool were screened for suppressors. The mapping-by-sequencing was carried out to isolate the suppressor gene as described by Hua et al. (2017). F_2 progenies from a cross of a suppressor mutant and *aca8 aca10* were used for mapping. Equal amounts of leaf tissues were collected from >50 plants

showing a suppressor phenotype and pooled for next-generation sequencing.

RNA-seq data analysis

For transcriptome analysis, total RNAs were extracted from tissues using Trizol (Invitrogen) according to the manufacturer's instructions. Total RNAs of 3 biological replicates were then processed at the Cornell Genomic Facility for 3′-RNA seq analysis on Illumina NextSeq500. The read count for each gene was obtained from the mapping result and normalized to CPM (count per million reads). DEGs were defined by FDR (false discovery rate) ≤ 0.001 and absolute value of $\log_2|\text{fold-change}| \geq 1$. DEGs were identified by DESeq2 (moderated estimation of fold change and dispersion for RNA-seq data) based on a pairwise comparison between the mutant and the wild type, setting q-value < 0.05 and $\log_2|\text{fold-change}| > 1$. The expression levels of these DEGs were subjected to CLUSTER and JAVA TREE for gene co-expression analysis (Hoon et al. 2004; Saldanha 2004). Heatmap was plotted by the TB tool (Chen et al. 2020) to visualize gene expression.

Pathogen growth assay

Pathogen growth assays were performed by dipping inoculation as previously described (Gou et al. 2015). Seedlings were grown for 14 d at 22 °C before inoculation. The amounts of bacteria in plants were analyzed at 1 h/0 d or 3 d post inoculation.

Confocal microscopy and calcium imaging

Confocal microscopy images were taken using the ZEISS LSM880 or LSM710 inverted confocal microscope equipped with the ZEISS software package. A 20× objective was used for imaging, and a zoom factor of 8-bit images was acquired with a frame size of 512×512 pixels. For the GCaMP6s indicator, GFP was excited at 488 nm and emission was collected at 500 to 545 nm. For the mCherry-GCaMP6f sensor, GFP was excited at 488 nm and emission was collected at 500 to 545 nm, while RFP was excited at 561 nm and emission was obtained at 580–630 nm (Weigand et al. 2021). For GCaMP6s, the gain of the detector was set at 1 and offset was set at 0, and the exposure time was set at 880 s for soil-grown plants and 960 s for hydroponic plants. The exposure time of mCherry-GCaMP6f was set at 800 s for RFP channel and GFP channel, the gain of the detector was set at 1, and the offset was set at 0. For the FRET-YC3.6 sensor, excitation was performed at 458 nm, and emissions were obtained at 470 to 490 nm for CFP and 530 to 570 nm for YFP. The exposure time of YC3.6 was set at 900 s for CFP Channel and 800 s for FRET-YFP; the gain of the detector was set at 2.4 and the offset was set at 0. Images were acquired using the same parameters within the same set of experiments. For GCaMP6s and YC3.6, samples were fixed on the slide and rested on a slide for at least 1 h before observation. For mCherry-GCaMP6f, samples were rested on a slide for at least 1 h followed by adapting to laser light for at least 1 h on the microscope stage before treatment and observation. Signal intensities from these reporters were measured using the image calculator tool in FIJI (Schindelin et al. 2012).

The 5th or 6th leaves from 3-wk-old plants grown in soil or 4-wk-old plants grown hydroponically were used for imaging unless specified otherwise. For minimizing physical perturbation of leaves during imaging, a modified imaging slide was made by placing 1 square coverslip on each end of the slide so that the sample can sit in the middle of the slide and a long coverslip can sit on the top of them. For *Pst* DC3000 treatment, plants were sprayed with a bacteria culture at optical density $OD_{600} = 0.05$, and leaves were collected and placed on the imaging slides. Samples were imaged at 1, 2, 3, 4, 5, 6, 7, 8, and 16 h after spray treatment. Treatment of cold, heat, and flg22 was done on leaves positioned on slides, and leaves were let to sit on slides for at least 1 h to allow calcium level to become steady before imaging and treatment. For cold or heat treatment, 200 µl ice or 42 °C water was added to the slide. For flg22 treatment, 2 µL of 10 mM flg22 was added to the 100 µL of H_2O on the imaging slide where the leaf sits to achieve a final concentration of 200 nM. Imaging frequency was set at 5 s for over 150 s (cold), 10 s for over 10 min (heat), or 1 min for over 35 min (flg22).

Cold and heat tolerance assays

For chilling treatment, plants were germinated and grown at 22 °C for 5 d and then grown at 10 °C until the wild-type plants set seeds. For heat treatment, plants of 2-wk growth at 22 °C were moved to and grown at 35 °C or 42 °C until the mutants died. Plants of different genotypes were planted side by side with each genotype occupying half a pot for phenotypic comparison. The heat and chilling tolerance tests were conducted for at least 3 times for the *aca8 aca10* mutant and 1 time for the *aca4 aca11* mutant. For survival status, live plants were assigned 1 and dead plants were assigned 0.

Stomatal closure assay

Stomatal closure assays were performed as previously described (Zeng et al. 2010) with slight modifications. Plants grown for 4 wk under a 12/12 h photoperiod at 22 °C were moved to 35 °C. Fully expanded leaves were collected before and after 1 d at 35 °C. Microscopic observation was done inside the walk-in growth chamber to keep all solutions and plant materials at the same temperature. Leaf epidermises were peeled, placed on ddH_2O, and observed under light microscopy within 2 to 3 h when no change in aperture was observed. At least 35 stomata from 10 leaves were imaged, and the aperture was measured using ImageJ software. The analysis was repeated for at least 3 times.

Leaf temperature and leaf conductance measurement

Leaf temperature was measured by using the MultispeQ V2.0 (Photosynq). Plants grown for 4 wk under a 12/12-h photoperiod at 22 °C were moved to 35 °C. The 5th or 6th leaves

were used for temperature measurement before and after 1 d at 35 °C.

Stomatal conductance was measured by using the SC-1 Leaf Porometer (Decagon Devices, Inc.). Plants grown at 22 °C for 4 wk under a 12/12-h photoperiod were moved to 35 °C. The 5th or 6th leaves were used for conductance measurement before and after 1 d at 35 °C.

Accession numbers

Sequence data from this article can be found in the GenBank/EMBL data libraries under accession numbers AT2G41560 (ACA4), AT5G57110 (ACA8), AT4G29900 (ACA10), AT3G57330 (ACA11), and AT1G19250 (FMO1).

Acknowledgments

We thank the Genomic Facility and Imaging Facility of Cornell Institute of Biotechnology for 3′-RNA seq analysis and confocal microscopy. We thank Destiny Meador and Chunmei Xue for assistance in material generation, Dr. Magdalena Julkowska for assistance in leaf temperature measurement, and Dr. Michael Allen Gore and Liam Wickes-Do for assistance in stomatal conductance measurement. We also thank Dr. Zhixue Wang for assistance in RNAseq data processing and Dr. Bo Li for assistance in microscope operation.

Supplemental data

The following materials are available in the online version of this article.

Supplemental Figure S1. $[Ca^{2+}]_{cyt}$ in response to external application of Ca^{2+}, and the suppression of autoimmunity in *aca8 aca10* by the *fmo1* mutation.

Supplemental Figure S2. Cluster and GO term enrichment analyses of differentially expressed genes (DEGs) among wild-type Col-0, *fmo1*, *aca8 aca10*, and *aca8 aca10 fmo1*.

Supplemental Figure S3. Growth and gene expression phenotypes of the wild-type Col-0, *aca8 aca10* under chilling.

Supplemental Figure S4. Growth phenotypes of wild-type Col-0, *fmo1*, *aca8 aca10*, and *aca8 aca10 fmo1* after 11 d at 42 °C.

Supplemental Figure S5. Cluster and GO term analysis based on DEGs of Col-0, *fmo1*, *aca8 aca10*, and *aca8 aca10 fmo1* plants under heat treatment.

Supplemental Movie S1. Ca^{2+} transient in response to flg22 stimulus in *aca8 aca10 fmo1*.

Supplemental Movie S2. Ca^{2+} transient in response to flg22 stimulus in Col-0.

Supplemental Movie S3. Ca^{2+} transient in response to cold stimulus in *aca8 aca10*.

Supplemental Movie S4. Ca^{2+} transient in response to cold stimulus in Col-0.

Supplemental Movie S5. Ca^{2+} transient in response to heat stimulus in *aca8 aca10*.

Supplemental Movie S6. Ca^{2+} transient in response to heat stimulus in Col-0.

Supplemental Data Set S1. Expression levels (in CPM) of SA-related genes in soil-grown plants of wild-type Col-0, *fmo1*, *aca8 aca10*, and *aca8 aca10 fmo1* at 22 °C.

Supplemental Data Set S2. Expression levels (in CPM) of SA-related genes in hydroponically grown plants of wild-type Col-0, *fmo1*, *aca8 aca10*, and *aca8 aca10 fmo1* at 22 °C and 10 °C.

Supplemental Data Set S3. Expression levels (in CPM) of HSF and HSP genes in soil-grown plants of wild-type Col-0, *fmo1*, *aca8 aca10*, and *aca8 aca10 fmo1* at 0, 1, and 7 d of 42 °C growth.

Supplemental Data Set S4. Primers used in construct generation and genotyping studies.

Funding

This work is supported by the National Science Foundation USA (IOS-1946174 to J.H. and NSF IOS 1656774 and IOS 2129234 to J.F.H.). We also acknowledge the funding support from NYSTEM (C029155) and NIH (S10OD018516 and S10RR025502) to the Imaging facility for the Zeiss LSM880 and LSM710 microscopes.

Conflict of interest statement. The authors declare no conflict of interest.

Data availability

All data relevant to the conclusions of this paper are included in the text and Supplemental data. Any additional data, reagents and transgenic lines are available upon request.

References

Ali R, Zielinski RE, Berkowitz GA. Expression of plant cyclic nucleotide-gated cation channels in yeast. J Exp Bot. 2005:**57**(1): 125–138. https://doi.org/10.1093/jxb/erj012

Alonso JM, Stepanova AN, Leisse TJ, Kim CJ, Chen H, Shinn P, Stevenson DK, Zimmerman J, Barajas P, Cheuk R. Genome-wide insertional mutagenesis of *Arabidopsis thaliana*. Science. 2003:**301**-(5633):653–657. https://doi.org/10.1126/science.1086391

Atwell S, Huang YS, Vilhjalmsson BJ, Willems G, Horton M, Li Y, Meng D, Platt A, Tarone AM, Hu TT, et al. Genome-wide association study of 107 phenotypes in *Arabidopsis thaliana* inbred lines. Nature. 2010:**465**(7298):627–631. https://doi.org/10.1038/nature08800

Behera S, Zhaolong X, Luoni L, Bonza MC, Doccula FG, De Michelis MI, Morris RJ, Schwarzlander M, Costa A. Cellular Ca^{2+} signals generate defined pH signatures in plants. Plant Cell. 2018:**30**(11): 2704–2719. https://doi.org/10.1105/tpc.18.00655

Bi G, Su M, Li N, Liang Y, Dang S, Xu J, Hu M, Wang J, Zou M, Deng Y, et al. The ZAR1 resistosome is a calcium-permeable channel triggering plant immune signaling. Cell. 2021:**184**(13):3528–3541. https://doi.org/10.1016/j.cell.2021.05.003

Bomblies K, Lempe J, Epple P, Warthmann N, Lanz C, Dangl JL, Weigel D. Autoimmune response as a mechanism for a Dobzhansky-Muller-type incompatibility syndrome in plants. PLoS Biol. 2007:**5**(9):e236. https://doi.org/10.1371/journal.pbio.0050236

Bonza MC, Morandini P, Luoni L, Geisler M, Palmgren MG, De Michelis MI. At-ACA8 encodes a plasma membrane-localized calcium-ATPase of Arabidopsis with a calmodulin-binding domain at the N terminus. Plant Physiol. 2000:**123**(4):1495–1506. https://doi.org/10.1104/pp.123.4.1495

Boursiac Y, Lee SM, Romanowsky S, Blank R, Sladek C, Chung WS, Harper JF. Disruption of the vacuolar calcium-ATPases in Arabidopsis results in the activation of a salicylic acid-dependent programmed cell death pathway. Plant Physiol. 2010:**154**(3): 1158–1171. https://doi.org/10.1104/pp.110.159038

Chen C, Chen H, Zhang Y, Thomas HR, Frank MH, He Y, Xia R. TBtools: an integrative toolkit developed for interactive analyses of big biological data. Mol Plant. 2020:**13**(8): 1194–1202. https://doi.org/10.1016/j.molp.2020.06.009

Chen TW, Wardill TJ, Sun Y, Pulver SR, Renninger SL, Baohan A, Schreiter ER, Kerr RA, Orger MB, Jayaraman V, et al. Ultrasensitive fluorescent proteins for imaging neuronal activity. Nature. 2013:**499-**(7458):295–300. https://doi.org/10.1038/nature12354

Choi WG, Hilleary R, Swanson SJ, Kim SH, Gilroy S. Rapid, long-distance electrical and calcium signaling in plants. Annu Rev Plant Biol. 2016:**67**(1):287–307. https://doi.org/10.1146/annurev-arplant-043015-112130

Costa A, Luoni L, Marrano CA, Hashimoto K, Koster P, Giacometti S, De Michelis MI, Kudla J, Bonza MC. Ca^{2+}-dependent phosphoregulation of the plasma membrane Ca^{2+}-ATPase ACA8 modulates stimulus-induced calcium signatures. J Exp Bot. 2017:**68**(12): 3215–3230. https://doi.org/10.1093/jxb/erx162

Cui Y, Lu S, Li Z, Cheng J, Hu P, Zhu T, Wang X, Jin M, Wang X, Li L, et al. CYCLIC NUCLEOTIDE-GATED ION CHANNELs 14 and 16 promote tolerance to heat and chilling in rice. Plant Physiol. 2020:**183**(4): 1794–1808. https://doi.org/10.1104/pp.20.00591

Curtis MD, Grossniklaus U. A gateway cloning vector set for high-throughput functional analysis of genes in planta. Plant Physiol. 2003:**133**(2):462–469. https://doi.org/10.1104/pp.103.027979

De Bigault DGA, Cacas JL. How very-long-chain fatty acids could signal stressful conditions in plants? Front Plant Sci. 2016:**7**:1490. https://doi.org/10.3389/fpls.2016.01490

Demidchik V, Shabala S, Isayenkov S, Cuin TA, Pottosin I. Calcium transport across plant membranes: mechanisms and functions. New Phytol. 2018:**220**(1):49–69. https://doi.org/10.1111/nph.15266

Dodd AN, Kudla J, Sanders D. The language of calcium signaling. Annu Rev Plant Biol. 2010:**61**(1):593–620. https://doi.org/10.1146/annurev-arplant-070109-104628

Fotouhi N, Fischer-Stettler M, Lenzoni G, Stolz S, Glauser G, Zeeman SC, Farmer EE. ACA Pumps maintain leaf excitability during herbivore onslaught. Curr Biol. 2022:**32**(11):2517–2528 e2516. https://doi.org/10.1016/j.cub.2022.03.059

Frei dit Frey N, Mbengue M, Kwaaitaal M, Nitsch L, Altenbach D, Haweker H, Lozano-Duran R, Njo MF, Beeckman T, Huettel B, et al. Plasma membrane calcium ATPases are important components of receptor-mediated signaling in plant immune responses and development. Plant Physiol. 2012:**159**(2):798–809. https://doi.org/10.1104/pp.111.192575

Garcia Bossi J, Kumar K, Barberini ML, Dominguez GD, Rondon Guerrero YDC, Marino-Buslje C, Obertello M, Muschietti JP, Estevez JM. The role of P-type IIA and P-type IIB Ca^{2+}-ATPases in plant development and growth. J Exp Bot. 2020:**71**(4):1239–1248. https://doi.org/10.1093/jxb/erz521

Geisler M, Frangne N, Gomès E, Martinoia E, Palmgren MG. The ACA4 gene of Arabidopsis encodes a vacuolar membrane calcium pump that improves salt tolerance in yeast. Plant Physiol. 2000:**124**(4):1814–1827. https://doi.org/10.1104/pp.124.4.1814

George L, Romanowsky SM, Harper JF, Sharrock RA. The ACA10 Ca^{2+}-ATPase regulates adult vegetative development and inflorescence architecture in Arabidopsis. Plant Physiol. 2008:**146**(2):716–728. https://doi.org/10.1104/pp.107.108118

Gou M, Zhang Z, Zhang N, Huang Q, Monaghan J, Yang H, Shi Z, Zipfel C, Hua J. Opposing effects on two phases of defense responses from concerted actions of HEAT SHOCK COGNATE70 and BONZAI1 in Arabidopsis. Plant Physiol. 2015:**169**(3):2304–2323. https://doi.org/10.1104/pp.15.00970

Harper JF, Hong B, Hwang I, Guo HQ, Stoddard R, Huang JF, Palmgren MG, Sze H. A novel calmodulin-regulated Ca^{2+}-ATPase (ACA2) from Arabidopsis with an N-terminal autoinhibitory domain. J Biol Chem. 1998:**273**(2):1099–1106. https://doi.org/10.1074/jbc.273.2.1099

Hartmann M, Zeier T, Bernsdorff F, Reichel-Deland V, Kim D, Hohmann M, Scholten N, Schuck S, Brautigam A, Holzel T, et al. Flavin monooxygenase-generated *N*-hydroxypipecolic acid is a critical element of plant systemic immunity. Cell. 2018:**173**(2): 456–469. https://doi.org/10.1016/j.cell.2018.02.049

Hilleary R, Paez-Valencia J, Vens C, Toyota M, Palmgren M, Gilroy S. Tonoplast-localized Ca^{2+} pumps regulate Ca^{2+} signals during pattern-triggered immunity in *Arabidopsis thaliana*. Proc Natl Acad Sci U S A. 2020:**117**(31):18849–18857. https://doi.org/10.1073/pnas.2004183117

Hong B. Identification of a calmodulin-regulated Ca^{2+}-ATPase in the endoplasmic Reticulum. Plant Physiol. 1999:**119**(4):1165–1176. https://doi.org/10.1104/pp.119.4.1165

Hoon MJLD, Imoto S, Nolan J, Miyano S. Open source clustering software. Bioinformatics. 2004:**20**(9):1453. https://doi.org/10.1093/bioinformatics/bth078

Hua J. Modulation of plant immunity by light, circadian rhythm, and temperature. Curr Opin Plant Biol. 2013:**16**(4):406–413. https://doi.org/10.1016/j.pbi.2013.06.017

Hua J, Wang S, Sun Q. Mapping and cloning of chemical induced mutations by whole-genome sequencing of bulked segregants. Methods Mol Biol. 2017:**1578**:285–289. https://doi.org/10.1007/978-1-4939-6859-6_24

Iwano M, Igarashi M, Tarutani Y, Kaothien-Nakayama P, Nakayama H, Moriyama H, Yakabe R, Entani T, Shimosato-Asano H, Ueki M, et al. A pollen coat-inducible autoinhibited Ca^{2+}-ATPase expressed in stigmatic papilla cells is required for compatible pollination in the Brassicaceae. Plant Cell. 2014:**26**(2):636–649. https://doi.org/10.1105/tpc.113.121350

Jacob P, Kim NH, Wu F, El-Kasmi F, Chi Y, Walton WG, Furzer OJ, Lietzan AD, Sunil S, Kempthorn K, et al. Plant "helper" immune receptors are Ca^{2+}-permeable nonselective cation channels. Science. 2021:**373**(6553):420–425. https://doi.org/10.1126/science.abg7917

Kim T-H, Böhmer M, Hu H, Nishimura N, Schroeder JI. Guard cell signal transduction network: advances in understanding abscisic acid, CO_2, and Ca^{2+} signaling. Annu Rev Plant Biol. 2010:**61**(1):561–591. https://doi.org/10.1146/annurev-arplant-042809-112226

Knight H, Trewavas AJ, Knight MR. Cold calcium signaling in Arabidopsis involves two cellular pools and a change in calcium signature after acclimation. Plant cell. 1996:**8**(3):489–503. https://doi.org/10.1105/tpc.8.3.489

Kudla J, Batistic O, Hashimoto K. Calcium signals: the lead currency of plant information processing. Plant Cell. 2010:**22**(3):541–563. https://doi.org/10.1105/tpc.109.072686

Lecourieux D, Ranjeva R, Pugin A. Calcium in plant defence-signalling pathways. New Phytol. 2006:**171**(2):249–269. https://doi.org/10.1111/j.1469-8137.2006.01777.x

Lee HJ, Seo PJ. Ca^{2+} talyzing initial responses to environmental stresses. Trends Plant Sci. 2021:**26**(8):849–870. https://doi.org/10.1016/j.tplants.2021.02.007

Lee SM, Kim HS, Han HJ, Moon BC, Kim CY, Harper JF, Chung WS. Identification of a calmodulin-regulated autoinhibited Ca^{2+}-ATPase (ACA11) that is localized to vacuole membranes in Arabidopsis. FEBS Lett. 2007:**581**(21):3943–3949. https://doi.org/10.1016/j.febslet.2007.07.023

Li Z, Liu H, Ding Z, Yan J, Yu H, Pan R, Hu J, Guan Y, Hua J. Low temperature enhances plant immunity via salicylic acid pathway genes

that are repressed by ethylene. Plant Physiol. 2020:**182**(1):626–639. https://doi.org/10.1104/pp.19.01130

Limonta M, Romanowsky S, Olivari C, Bonza MC, Luoni L, Rosenberg A, Harper JF, De Michelis MI. ACA12 is a deregulated isoform of plasma membrane Ca^{2+}-ATPase of *Arabidopsis thaliana*. Plant Mol Biol. 2014:**84**(4–5):387–397. https://doi.org/10.1007/s11103-013-0138-9

Liu KH, Niu Y, Konishi M, Wu Y, Du H, Sun Chung H, Li L, Boudsocq M, McCormack M, Maekawa S, et al. Discovery of nitrate-CPK-NLP signalling in central nutrient-growth networks. Nature. 2017:**545**-(7654):311–316. https://doi.org/10.1038/nature22077

Luan S, Wang C. Calcium signaling mechanisms across kingdoms. Annu Rev Cell Dev Biol. 2021:**37**(1):311–340. https://doi.org/10.1146/annurev-cellbio-120219-035210

Malmström S, Askerlund P, Palmgren MG. A calmodulin-stimulated Ca^{2+}-ATPase from plant vacuolar membranes with a putative regulatory domain at its N-terminus. FEBS Lett. 1997:**400**(3):324–328. https://doi.org/10.1016/S0014-5793(96)01448-2

Nagai T, Yamada S, Tominaga T, Ichikawa M, Miyawaki A. Expanded dynamic range of fluorescent indicators for Ca^{2+} by circularly permuted yellow fluorescent proteins. Proc Natl Acad Sci U S A. 2004:**101**-(29):10554–10559. https://doi.org/10.1073/pnas.0400417101

Rahmati Ishka M, Brown E, Rosenberg A, Romanowsky S, Davis JA, Choi WG, Harper JF. Arabidopsis Ca^{2+}-ATPases 1, 2, and 7 in the endoplasmic reticulum contribute to growth and pollen fitness. Plant Physiol. 2021:**185**(4):1966–1985. https://doi.org/10.1093/plphys/kiab021

Saldanha AJ. Java treeview—extensible visualization of microarray data. Bioinformatics. 2004:**20**(17):3246–3248. https://doi.org/10.1093/bioinformatics/bth349

Schindelin J, Arganda-Carreras I, Frise E, Kaynig V, Longair M, Pietzsch T, Preibisch S, Rueden C, Saalfeld S, Schmid B. Fiji: an open-source platform for biological-image analysis. Nat Methods. 2012:**9**(7):676–682. https://doi.org/10.1038/nmeth.2019

Schiott M, Palmgren MG. Two plant Ca^{2+} pumps expressed in stomatal guard cells show opposite expression patterns during cold stress. Physiol Plant. 2005:**124**(2):278–283. https://doi.org/10.1111/j.1399-3054.2005.00512.x

Schiott M, Romanowsky SM, Baekgaard L, Jakobsen MK, Palmgren MG, Harper JF. A plant plasma membrane Ca^{2+} pump is required for normal pollen tube growth and fertilization. Proc Natl Acad Sci U S A. 2004:**101**(25):9502–9507. https://doi.org/10.1073/pnas.0401542101

Shigaki T, Hirschi KD. Diverse functions and molecular properties emerging for CAX cation/H^+ exchangers in plants. Plant Biol (Stuttg). 2006:**8**(4):419–429. https://doi.org/10.1055/s-2006-923950

Spalding EP, Harper JF. The ins and outs of cellular Ca^{2+} transport. Curr Opin Plant Biol. 2011:**14**(6):715–720. https://doi.org/10.1016/j.pbi.2011.08.001

Sze H, Liang F, Hwang I, Curran AC, Harper JF. Diversity and regulation of plant Ca^{2+} pumps: insights from expression in yeast. Annu Rev Plant Phys. 2000:**51**(1):433–462. https://doi.org/10.1146/annurev.arplant.51.1.433

Tandonnet S, Torres TT. Traditional versus 3′ RNA-seq in a non-model species. Genom Data. 2017:**11**(9):9–16. https://doi.org/10.1016/j.gdata.2016.11.002

Thor K, Jiang S, Michard E, George J, Scherzer S, Huang S, Dindas J, Derbyshire P, Leitao N, DeFalco TA, et al. The calcium-permeable channel OSCA1.3 regulates plant stomatal immunity. Nature. 2020:**585**(7826):569–573. https://doi.org/10.1038/s41586-020-2702-1

Tian W, Hou C, Ren Z, Wang C, Zhao F, Dahlbeck D, Hu S, Zhang L, Niu Q, Li L, et al. A calmodulin-gated calcium channel links pathogen patterns to plant immunity. Nature. 2019:**572**(7767):131–135. https://doi.org/10.1038/s41586-019-1413-y

Tidow H, Poulsen LR, Andreeva A, Knudsen M, Hein KL, Wiuf C, Palmgren MG, Nissen P. A bimodular mechanism of calcium control in eukaryotes. Nature. 2012:**491**(7424):468–472. https://doi.org/10.1038/nature11539

Toyota M, Spencer D, Sawai-Toyota S, Wang J, Zhang T, Koo AJ, Howe GA, Gilroy S. Glutamate triggers long-distance, calcium-based plant defense signaling. Science. 2018:**361**(6407):1112–1115. https://doi.org/10.1126/science.aat7744

Wang Y, Zhang Y, Wang Z, Zhang X, Yang S. A missense mutation in CHS1, a TIR-NB protein, induces chilling sensitivity in Arabidopsis. Plant J. 2013:**75**(4):553–565. https://doi.org/10.1111/tpj.12232

Weigand C, Kim SH, Brown E, Medina E, Mares M 3rd, Miller G, Harper JF, Choi WG. A ratiometric calcium reporter CGf reveals calcium dynamics both in the single cell and whole plant levels under heat stress. Front Plant Sci. 2021:**12**:777975. https://doi.org/10.3389/fpls.2021.777975

Wildermuth MC, Dewdney J, Wu G, Ausubel FM. Isochorismate synthase is required to synthesize salicylic acid for plant defence. Nature. 2001:**414**(6863):562–565. https://doi.org/10.1038/35107108

Yang DL, Shi Z, Bao Y, Yan J, Yang Z, Yu H, Li Y, Gou M, Wang S, Zou B, et al. Calcium pumps and interacting BON1 protein modulate calcium signature, stomatal closure, and plant immunity. Plant Physiol. 2017:**175**(1):424–437. https://doi.org/10.1104/pp.17.00495

Yu H, Yan J, Du X, Hua J. Overlapping and differential roles of plasma membrane calcium ATPases in Arabidopsis growth and environmental responses. J Exp Bot. 2018:**69**(10):2693–2703. https://doi.org/10.1093/jxb/ery073

Yuan F, Yang H, Xue Y, Kong D, Ye R, Li C, Zhang J, Theprungsirikul L, Shrift T, Krichilsky B, et al. OSCA1 mediates osmotic-stress-evoked Ca^{2+} increases vital for osmosensing in Arabidopsis. Nature. 2014:**514**-(7522):367–371. https://doi.org/10.1038/nature13593

Zeng W, Melotto M, He SY. Plant stomata: a checkpoint of host immunity and pathogen virulence. Curr Opin Biotechnol. 2010:**21**(5):599–603. https://doi.org/10.1016/j.copbio.2010.05.006

Zhi Qi NRS, Spalding EP. Calcium entry mediated by GLR3.3, an Arabidopsis glutamate receptor with a broad agonist profile. Plant Physiol. 2006:**142**(3):963–971. https://doi.org/10.1104/pp.106.088989